A General Two-Phase Markov Chain Monte Carlo Approach for Constrained Design Optimization: Application to Stochastic Structural Optimization

H. Jensen[1,3], D. Jerez[2], and M. Beer[2,3,4]

[1] *Department of Civil Engineering, Federico Santa Maria Technical University, Valparaiso, Chile*

[2] *Institute for Risk and Reliability, Leibniz Universität Hannover, 30167 Hannover, Germany.*

[3] *International Joint Research Center for Engineering Reliability and Stochastic Mechanics, Tongji University, Shanghai 200092, China.*

[4] *Institute for Risk and Uncertainty and School of Engineering, University of Liverpool, Liverpool L69 7ZF, U.*

Abstract

This contribution presents a general approach for solving structural design problems formulated as a class of nonlinear constrained optimization problems. A Two-Phase approach based on Bayesian model updating is considered for obtaining the optimal designs. Phase I generates samples (designs) uniformly distributed over the feasible design space, while Phase II obtains a set of designs lying in the vicinity of the optimal solution set. The equivalent model updating problem is solved by the transitional Markov chain Monte Carlo method. The proposed constraint-handling approach is direct and does not require special constraint-handling techniques. The population-based stochastic optimization algorithm generates a set of nearly optimal solutions uniformly distributed over the vicinity of the optimal solution set. The set of optimal solutions provides valuable sensitivity information. In addition, the proposed scheme is a useful tool for exploration of complex feasible design spaces. The general approach is applied to an important class of problems. Specifically, reliability-based design optimization of structural dynamical systems under stochastic excitation. Numerical examples are presented to evaluate the effectiveness of the proposed design scheme.

Keywords: Constrained optimization, Feasible design space, Meta-models, Markov sampling method, Reliability-based design, Stochastic optimization.

*H.A. Jensen - hector.jensen@usm.cl

1. Introduction

Structural optimization by means of mathematical programming techniques has been widely accepted as a viable tool for engineering design. The majority of engineering problems involve constrained optimization. The problem is generally that of minimizing a cost function or maximizing a utility function. The constraints are generally those on resources or demand levels. Thus, the optimal design can be regarded as the best feasible design according to a preselected quantitative measure of effectiveness. Due to the practical importance of this class of problems, the development of efficient constrained optimization algorithms has been an important area of research in engineering design [1, 2]. Generally, constrained optimization algorithms are based on standard optimization schemes or stochastic search algorithms. Though, traditional algorithms are well documented in the literature and extensively used in engineering design, final solutions or designs are usually local optima. In this regard, several global optimization algorithms have been devised, including genetic algorithms, simulated annealing, multi-start algorithms, ant colony optimization, particle swarm optimization, annealing evolutionary stochastic approximation Monte Carlo, etc. [3, 4, 5, 6, 7]. One important issue associated with constrained optimization is constraint-handling [8, 9, 10]. A number of strategies have been suggested in the context of specific stochastic optimization algorithms such as evolutionary algorithms [11], simulated annealing [12], particle swarm optimization [13], and subset simulation-based algorithm [14]. Although the previous stochastic optimization algorithms have been applied in a number of constrained optimization problems, there is still room for further developments in this area, specially when dealing with involved structural models and complex systems.

In the previous context, it is the objective of this contribution to present a framework for solving structural design problems formulated as nonlinear constrained optimization problems. First, the optimization problem is set into the framework of a Two-Phase Bayesian model updating problem. Phase I generates designs uniformly distributed over the feasible design space, while Phase II obtains a set of designs lying in the vicinity of the optimal solution set. The corresponding Bayesian model updating problem is solved by the transitional Markov chain Monte Carlo method [15, 16]. The methodology can efficiently explore the sensitivity of final designs and constraints with respect to the design variables in the vicinity of the optimal design. The proposed constraint-handling approach is direct and does not require special constraint-handling techniques. Actually, the same framework for obtaining samples in the vicinity of the optimal solution set is used for

obtaining samples in the feasible design space. The proposed Two-Phase approach can be viewed as a generalization of the work presented in [17]. In that work, an optimization scheme was proposed for solving unconstrained optimization problems with applications to performance-based design. Moreover, this work can be interpreted as an additional area of application of simulation-based Bayesian model updating techniques. Though the proposed approach can handle general constrained optimization problems, the focus of this contribution is on the reliability-based design optimization of structural dynamical systems under stochastic excitation. It is noted that solving this class of problems involves estimating the system reliability at different designs during the optimization process which is well-known to be very challenging. Then, an efficient and effective solution of this class of problems is important from the practical viewpoint.

The organization of the paper is as follows. Section 2 describes the class of nonlinear constrained optimization problems to be considered in the present contribution. The main ideas of the proposed Two-Phase scheme are discussed in Section 3. Several aspects associated with the implementation of the proposed optimization scheme are addressed in Section 4. Four numerical examples are provided in Section 5. The paper closes with some conclusions and future research efforts.

2. Description of the Problem

Consider the following inequality-constrained non-linear optimization problem

$$\begin{aligned} \text{Min}_{\mathbf{x}} \quad & c(\mathbf{x}) \\ \text{s.t.} \quad & r_i(\mathbf{x}) \leq 1 \ , \ i = 1, ..., n_r \\ & \mathbf{x} \in \mathbf{X} \end{aligned} \tag{1}$$

where $\mathbf{x} \in \mathbf{X} \subset R^{n_d}, x_i, i = 1, ..., n_d,$ is the vector of design variables with side constraints $x_i^l \leq x_i \leq x_i^u$, $c(\mathbf{x})$ is the objective or cost function, and $r_i(\mathbf{x}) \leq 1 \ , \ i = 1, ..., n_r$ are general design constraints. Note that in the present formulation the set of design variables are assumed to be continuous. The objective function $c(\mathbf{x})$ can be defined in terms of initial, construction, repair or downtime costs, structural weight, general cost functions, expected performance measures, etc. Moreover, the constraints may be associated with design requirements such as geometric conditions, material cost components, demand levels, design specifications characterized by means

of different performance measures, including reliability measures. Thus, the above formulation is quite general since different optimization formulations can be considered.

3. Optimization Strategy

3.1. Basic background

An approach based on the transitional Markov chain Monte Carlo method (TMCMC) [15, 18] is considered for solving the constrained optimization problem. The TMCMC method, which corresponds to a class of sequential particle filter methods, has proved to be quite effective in a number of Bayesian model updating problems [15, 19, 20, 21, 22]. In fact, this sampling method is capable of populating the region of interest even in challenging model updating problems. In what follows, and for completeness, some of the fundamental ideas of the TMCMC method are reviewed. In this context, it is assumed that the structural model is characterized in terms of a set of model parameters $\boldsymbol{\theta}$. The objective of Bayesian model updating is to estimate the posterior probability density function of $\boldsymbol{\theta}$, $f_D(\boldsymbol{\theta})$, given some data D. The method relies on the construction of a series of non-normalized intermediate distributions, $f_{D_j}(\boldsymbol{\theta})$, defined as

$$f_{D_j}(\boldsymbol{\theta}) \propto \; l_D(\boldsymbol{\theta})^{\alpha_j} f(\boldsymbol{\theta}) \; , \quad j = 0, 1, ..., M \tag{2}$$

where $l_D(\boldsymbol{\theta})$ represents the likelihood of observing the data D for a given value of the model parameters $\boldsymbol{\theta}$, $f(\boldsymbol{\theta})$ is the prior distribution representing the initial belief or information about the distribution of $\boldsymbol{\theta}$, and α_j is a parameter that increases monotonically with j such that $\alpha_0 = 0$, and $\alpha_M = 1$. In the first step ($j = 0$), the samples are generated from the prior distribution, while in the last stage ($j = M$) the samples are asymptotically distributed as $f_D(\boldsymbol{\theta})$. Due to the nature and annealing property of the TMCMC method, the samples at the last stage of the updating process tend to maximize the likelihood function $l_D(\boldsymbol{\theta})$. This feature of the TMCMC method establishes a connection between Bayesian model updating problems and the solution of the optimization problem defined in Eq. (1). In what follows, such connection is discussed in detail.

3.2. Preliminary observations

It is noted that finding the minimum of the objective function $c(\mathbf{x})$ is equivalent to find the maximum of the function $\exp(-c(\mathbf{x})/T)$, for any given value of $T > 0$ [4]. In connection with

this result, and treating the design variables as random variables uniformly distributed over the feasible design space $\mathbf{X}_{\text{feasible}}$, where

$$\mathbf{X}_{\text{feasible}} = \{\mathbf{x} \in \mathbf{X} : r_i(\mathbf{x}) \leq 1 \ , \ i = 1, ..., n_r\} \, , \tag{3}$$

define the non-normalized auxiliary distribution

$$f_T(\mathbf{x}) \propto \ \exp\left(-\frac{c(\mathbf{x})}{T}\right) \ \ I_{\mathbf{X}_{\text{feasible}}}(\mathbf{x}) \tag{4}$$

where $I_{\mathbf{X}_{\text{feasible}}}(\mathbf{x})$ is the indicator function of the feasible design space $\mathbf{X}_{\text{feasible}}$, that is, $I_{\mathbf{X}_{\text{feasible}}}(\mathbf{x}) = 1$, for $\mathbf{x} \in \mathbf{X}_{\text{feasible}}$, and $I_{\mathbf{X}_{\text{feasible}}}(\mathbf{x}) = 0$, otherwise. It is seen that $f_T(\mathbf{x})$ becomes flatter as the parameter T increases. In fact, $f_T(\mathbf{x})$ is proportional to $I_{\mathbf{X}_{\text{feasible}}}(\mathbf{x})$ as $T \to \infty$. Moreover, as T decreases and tends to zero, the distribution $f_T(\mathbf{x})$ becomes spikier, and it puts more and more of its probability mass into the set that maximizes the function $\exp(-c(\mathbf{x})/T)$, and therefore the corresponding samples minimize the objective function $c(\mathbf{x})$ (optimal solutions set $\mathbf{X}^*$). Thus, a sample drawn from $f_T(\mathbf{x})$ will be in the vicinity of the optimal solutions set $\mathbf{X}^*$ with a very high probability when T converges to zero [23, 24]. Note that in the previous setting, the design variables are artificially treated as random variables as previously pointed out. Such uncertainty is just a tool for setting the optimization problem in the framework of a Bayesian model updating problem.

3.3. Approach: General Idea

Based on the previous observations, the basic features of the TMCMC method, and some of the ideas suggested in [17, 23, 24], define a sequence of non-normalized intermediate distributions as

$$f_{T_0}(\mathbf{x}) \propto \ I_{\mathbf{X}_{\text{feasible}}}(\mathbf{x}) \tag{5}$$

$$f_{T_j}(\mathbf{x}) \propto \ \exp\left(-\frac{c(\mathbf{x})}{T_j}\right) \ \ I_{\mathbf{X}_{\text{feasible}}}(\mathbf{x}) \quad , \quad j = 1, 2, ... \tag{6}$$

where $\infty = T_0 > T_1 > ... > T_j > ...$ is a sequence of monotonically decreasing parameters with $T_j \to 0$ as $j \to \infty$. In the context of Section 3.1, the design variables $\mathbf{x}$ correspond to the model parameters $\boldsymbol{\theta}$, the function $\exp(-c(\mathbf{x}))$ takes the role of the likelihood function $l_D(\boldsymbol{\theta})$ with $T_j = 1/\alpha_j$, while $I_{\mathbf{X}_{\text{feasible}}}(\mathbf{x})$ represents the non-normalized prior distribution. Note that the

corresponding prior normalized distribution is the uniform distribution, $U_{\mathbf{X}_{\text{feasible}}}(\mathbf{x})$, defined over the feasible design space. In the framework of the TMCMC method, the parameters $T_j, j = 1, 2, ...$ are constructed adaptively in such a way that the distributions $f_{T_j}(\mathbf{x})$ and $f_{T_{j+1}}(\mathbf{x})$ be similar by using different criteria [15, 25, 26].

The iteration starts with the generation of samples (designs) $\mathbf{x}_1^0, ..., \mathbf{x}_n^0$ from $I_{\mathbf{X}_{\text{feasible}}}(\mathbf{x})$ in order to populate the feasible design space. The samples at stage $j + 1$, i.e. $\mathbf{x}_1^{j+1}, ..., \mathbf{x}_n^{j+1}$, $j = 0, 1, ...$, are obtained by generating Markov chains as in the TMCMC method. The procedure is repeated until a stopping criterion is satisfied. The idea of the method is to iterate until the parameter T_{j+1} is small enough so that the corresponding samples $\mathbf{x}_1^{j+1}, ..., \mathbf{x}_n^{j+1}$ are approximately uniformly distributed over the optimal solution set $\mathbf{X}^*$. The samples at the optimal solutions set represent possible designs with similar values of the objective function $c(\mathbf{x})$. If a single optimal solution is needed, a possible choice based on the samples $\mathbf{x}_1^{j+1}, ..., \mathbf{x}_n^{j+1}$ is given by $\mathbf{x}^*$, such that $c(\mathbf{x}^*) = \min_{i=1,...,n} c(\mathbf{x}_i^{j+1})$. The reader is referred to [15, 16, 18] for a detailed implementation of the TMCMC method.

3.4. Approach: Phase I

It is seen that the proposed approach requires drawing samples uniformly distributed over the feasible design space $\mathbf{X}_{\text{feasible}}$, that is, designs that verify the side constraints, i.e., $\mathbf{x} \in \mathbf{X}$, and the constraints $r_i(\mathbf{x}) \leq 1$, $i = 1, ..., n_r$. This is an involved task since the feasible design space, which is not known in advance, could be quite complex. To overcome this difficulty, the following scheme is devised. Consider the following auxiliary unconstrained optimization problem defined in terms of the constraint functions of the original constrained problem given in Eq. (1)

$$\begin{aligned} &\text{Min}_{\mathbf{x}} \quad h(\mathbf{x}) \\ &\text{s.t.} \quad \mathbf{x} \in \mathbf{X} \end{aligned} \tag{7}$$

where $h(\mathbf{x})$ is an auxiliary objective function defined as

$$h(\mathbf{x}) = \begin{cases} \max_i \{r_i(\mathbf{x})\} & \text{if } \exists\ i :\ r_i(\mathbf{x}) > 1 \\ 1 & \text{if } \forall\ i\ ,\ r_i(\mathbf{x}) \leq 1 \end{cases} \tag{8}$$

where $i = 1, ..., n_r$. Based on the definition of the auxiliary objective function, it is clear that the minimum value of $h(\mathbf{x})$ is equal to 1, while the corresponding optimum solution set, $\mathbf{X}_h^*$, is given by

$$\mathbf{X}_h^* = \{\mathbf{x} \in \mathbf{X} : r_i(\mathbf{x}) \leq 1, \quad i = 1, ..., n_r\} \tag{9}$$

In other words, the optimum solution set of the auxiliary unconstrained optimization problem is equal to the feasible design space, $\mathbf{X}_{\text{feasible}}$, of the original constrained optimization problem (1). Then, the solution of the unconstrained optimization problem (7) provides a set of designs in the feasible design space. Note that the auxiliary optimization problem can be solved as indicated in Section 3.3, with a sequence of non-normalized intermediate distributions defined as

$$f_{T_0}(\mathbf{x}) \propto \; U_{\mathbf{X}}(\mathbf{x}) \tag{10}$$

$$f_{T_j}(\mathbf{x}) \propto \; \exp\left(-\frac{h(\mathbf{x})}{T_j}\right) \; U_{\mathbf{X}}(\mathbf{x}) \quad , \quad j = 1, 2, ... \tag{11}$$

where $U_{\mathbf{X}}(\mathbf{x})$ is the uniform distribution defined over $\mathbf{X}$. Recall that $\mathbf{X}$ is the set that defines the side constraints of the design variables. It is easy to show that all feasible samples generated during the different stages of Phase I are uniformly distributed over $\mathbf{X}_{\text{feasible}}$. Then, the sampling process can be stopped if the total number of feasible samples (designs) reaches a certain pre-determined value n_{target}.

3.5. Approach: Phase II

The goal of Phase II is to obtain a set of designs lying in the vicinity of the optimal solution set $\mathbf{X}^*$, associated with the constrained optimization problem (1). To this end, and in the context of the approach proposed in Section 3.3, the samples at the initial stage of the updating process, which should be uniformly distributed over the feasible design space $\mathbf{X}_{\text{feasible}}$, are the ones obtained from Phase I. Thus, the Two-Phase framework allows the solution of the general constrained design problem formulated in Eq. (1). It is noted that the same framework for obtaining samples in the vicinity of the optimal solution set, that is, Phase II, is used for obtaining samples in the feasible design space, i.e., Phase I. Thus, special constraint-handling techniques are not necessary.

4. Implementation Aspects

4.1. Updating Process

The actual updating process is performed in an underlying normal space $\mathbf{Y} \subset R^{n_d}$ of independent standard normal variables. The mapping between the spaces $\mathbf{Y}$ and $\mathbf{X}$, i.e., $\mathbf{x} = \mathbf{x}(\mathbf{y})$

is given by $x_i = x_i(y_i) = x_i^l + \Phi(y_i)(x_i^u - x_i^l), i = 1, ..., n_d$, where $\Phi(\cdot)$ is the standard normal cumulative univariate distribution function. Validation calculations have shown that performing the updating process in the underlying standard normal space has some numerical advantages due to normalization and boundedness issues [16, 17]. Note that, however, an implementation of the updating process in the physical design space $\mathbf{X}$ is also possible. Once the problem is set into the space of independent standard normal variables, and based on some of the ideas suggested in [17, 23, 24], the Two-Phase scheme is implemented as follows.

4.2. Pseudo-Code: Phase I

The following steps are involved in Phase I.

1) Initial stage

Set $j = 0$ ($T_0 = \infty$), and generate samples $\{\mathbf{y}_1^0, \ldots, \mathbf{y}_{n_0}^0\}$ in the underlying standard normal space by Monte Carlo simulation. Compute the auxiliary objective function values $\{h(\mathbf{x}(\mathbf{y}_1^0)), \ldots, h(\mathbf{x}(\mathbf{y}_{n_0}^0))\}$.

2) Determination of T_{j+1}

The criterion to select T_{j+1} is based on the effective sample size technique [25, 26]. This technique measures how similar the non-normalized intermediate distribution f_{T_j} is to $f_{T_{j+1}}$. An estimator of the effective sample size, n_{eff}, is given by $\hat{n}_{eff} = 1/\sum_{i=1}^{n_j} \left(\bar{w}_i^j\right)^2$, where n_j is the number of samples at stage j, and $\bar{w}_i^j$ represents the normalized importance weight of the sample $\mathbf{y}_i^j$ (see Step 3). Based on this estimator, it follows that if the distributions are alike, the effective sample size is close to n_j, while n_{eff} is a small number if the distributions are different. The value of T_{j+1} is chosen by imposing the condition $n_{eff} = \nu n_j$ where $\nu \in (0, 1)$ is a user-defined parameter. This condition gives the following nonlinear equation for T_{j+1}

$$\frac{\sum_{i=1}^{n_j} \exp\left(-2h(\mathbf{x}(\mathbf{y}_i^j))\left[\frac{1}{T_{j+1}} - \frac{1}{T_j}\right]\right)}{\left(\sum_{i=1}^{n_j} \exp\left(-h(\mathbf{x}(\mathbf{y}_i^j))\left[\frac{1}{T_{j+1}} - \frac{1}{T_j}\right]\right)\right)^2} = \frac{1}{\nu n_j} \tag{12}$$

The previous nonlinear equation can be solved by any suitable numerical technique.

3) Computation of importance weights

Once the parameter T_{j+1} has been determined, compute the importance weights w_i^j of the samples as

$$w_i^j = \frac{f_{T_{j+1}}(\mathbf{x}(\mathbf{y}_i^j))}{f_{T_j}(\mathbf{x}(\mathbf{y}_i^j))} = \exp\left(-h(\mathbf{x}(\mathbf{y}_i^j))\left[\frac{1}{T_{j+1}} - \frac{1}{T_j}\right]\right), \quad i = 1, \ldots, n_j \tag{13}$$

and the corresponding normalized importance weights $\bar{w}_i^j = w_i^j / \sum_{p=1}^{n_j} w_p^j, \quad i = 1, \ldots, n_j$.

4) Generation of samples for stage $j+1$

The samples from $f_{T_{j+1}}$ are based on the samples from f_{T_j}, and according to the TMCMC scheme, they are obtained by generating Markov chains where the lead samples are selected from the distribution f_{T_j}. The lead sample of the Markov chain is a sample from the previous step, e.g. $\mathbf{y}_l^j$, which is selected according to its normalized weight [15]. Each Markov chain is generated by applying the Metropolis-Hastings algorithm [27, 28]. The corresponding proposal probability density function is a Gaussian distribution centered at the previous sample of the chain and with covariance matrix $\mathbf{\Sigma}_j$ equal to a scaled version of the estimate covariance matrix of the current intermediate distribution f_{T_j}, that is, $\mathbf{\Sigma}_j = \beta^2 \sum_{i=1}^{n_j} \bar{w}_i^j \left(\mathbf{y}_i^j - \bar{\mathbf{y}}^j\right)\left(\mathbf{y}_i^j - \bar{\mathbf{y}}^j\right)^T$, $\bar{\mathbf{y}}^j = \sum_{i=1}^{n_j} \bar{w}_i^j \mathbf{y}_i^j$, where β^2 is a parameter that can be chosen according to different criteria. For example, it can be defined directly by the user or by an adaptive scheme based on the acceptance rate of the sampling process [16, 29].

5) Stopping criterion

At stage $j+1$, identify all samples $\{\mathbf{y}_1, \ldots, \mathbf{y}_m\}$ generated during the previous stages of the updating process, such that $h(\mathbf{x}(\mathbf{y}_i)) = 1, i = 1, ..., m$. If $m \geq n_{\text{target}}$ stop the process and continue to Phase II where the samples $\{\mathbf{y}_1, \ldots, \mathbf{y}_m\}$ are used at the initial stage. If $m < n_{\text{target}}$, return to step 2 with $j \leftarrow j+1$.

4.3. Pseudo-Code: Phase II

The following steps are involved in Phase II.

1) Initial stage

Set $j = 0$ ($T_0 = \infty$). The initial samples of the process, uniformly distributed over the feasible design space $\mathbf{X}_{\text{feasible}}$, are the designs obtained during Phase I. Compute the objective function values $\{c(\mathbf{x}(\mathbf{y}_1^0)), \ldots, c(\mathbf{x}(\mathbf{y}_{n_0}^0))\}$, where $n_0 = m$. Next, compute the corresponding coefficient of variation (c.o.v.) of these samples as

$$\delta_0 = \sqrt{\frac{1}{n_0 - 1}\sum_{i=1}^{n_0}\left[c(\mathbf{x}(\mathbf{y}_i^0)) - \left(\frac{1}{n_0}\sum_{p=1}^{n_0} c(\mathbf{x}(\mathbf{y}_p^0))\right)\right]^2} \Bigg/ \frac{1}{n_0}\sum_{p=1}^{n_0} c(\mathbf{x}(\mathbf{y}_p^0)) \tag{14}$$

2) Initial information for stopping criterion

Set $\delta_{target} = \gamma\delta_0$, where γ is a user-defined parameter, and δ_{target} is the target c.o.v. of the objective function values. Alternatively, the stopping criterion can be defined in terms of a pre-determined maximum number of stages $j_{\max}$.

3) Determination of T_{j+1}

As in Phase I, the criterion to select T_{j+1} is based on the effective sample size technique [25, 26]. Thus, the value of T_{j+1} is chosen to satisfy the nonlinear equation

$$\frac{\sum_{i=1}^{n_j} \exp\left(-2c(\mathbf{x}(\mathbf{y}_i^j))\left[\frac{1}{T_{j+1}} - \frac{1}{T_j}\right]\right)}{\left(\sum_{i=1}^{n_j} \exp\left(-c(\mathbf{x}(\mathbf{y}_i^j))\left[\frac{1}{T_{j+1}} - \frac{1}{T_j}\right]\right)\right)^2} = \frac{1}{\nu n_j} \tag{15}$$

where n_j is the number of samples at stage j, and $\nu \in (0,1)$ is as before, a user-defined parameter.

4) Computation of importance weights

The importance weight w_i^j of the sample $\mathbf{y}_i^j$ is defined as

$$w_i^j = \exp\left(-c(\mathbf{x}(\mathbf{y}_i^j))\left[\frac{1}{T_{j+1}} - \frac{1}{T_j}\right]\right), \quad i = 1, \ldots, n_j \tag{16}$$

with normalized importance weight $\bar{w}_i^j = w_i^j / \sum_{p=1}^{n_j} w_p^j, \quad i = 1, \ldots, n_j$.

5) Generation of samples for stage $j+1$

The generation of samples at each step proceeds in a similar manner as in step 4 of Phase I. However, in this case, the candidate sample generated in the context of the Metropolis-Hasting algorithm should belong to the feasible design space $\mathbf{X}_{\text{feasible}}$. If not, the sample is rejected.

6) Stopping criterion

Compute the sample c.o.v. of the objective function values at the $(j+1)$-th stage, δ_{j+1}, as

$$\delta_{j+1} = \sqrt{\frac{1}{n_{j+1}-1}\sum_{i=1}^{n_{j+1}}\left(c(\mathbf{x}(\mathbf{y}_i^{j+1})) - \left[\frac{1}{n_{j+1}}\sum_{p=1}^{n_{j+1}} c(\mathbf{x}(\mathbf{y}_p^{j+1}))\right]\right)^2} \Bigg/ \frac{1}{n_{j+1}}\sum_{p=1}^{n_{j+1}} c(\mathbf{x}(\mathbf{y}_p^{j+1})) \tag{17}$$

If $\delta_{j+1} \geq \delta_{target}$, set $j \leftarrow j+1$ and return to Step 3. Otherwise, set $M = j+1$ and stop the process. Obtain the sample-based optimum design $\mathbf{x}^*$, and the corresponding objective function value as $c(\mathbf{x}^*) = \min_{i=1,\ldots,n_M} c(\mathbf{x}(\mathbf{y}_i^M))$. Alternatively, the optimization process can be stopped if

a maximum number of stages $j_{\max}$ has been reached as indicated in step 2. It is noted that other stopping criteria could be also implemented.

4.4. Practical Observations

As previously pointed out, all feasible samples generated during Phase I are used at the initial stage of Phase II. Additionally, these samples can also be used to explore the feasible design space in a direct manner. This information can give valuable insight into the optimization problem, especially when the design variables exhibit a complex interaction between them. Moreover, the information from the uniformly distributed samples could also be used in connection with other optimization techniques. For example, the best design among the samples generated in Phase I can be used as the initial design in gradient-based optimization schemes such as interior point algorithms. Finally, it is noted that the best solution from Phase I could also be used as an approximation of the solution to the original optimization problem (1). In this case, the accuracy of the solution should be studied in detail.

4.5. Additional Implementation Issues

High performance computing (HPC) techniques at the computer hardware level can be considered for increasing the computational efficiency of the proposed Two-Phase approach. In fact, recall that the proposed optimization process, which is based on the TMCMC method, is suitable for a parallel implementation in a HPC environment. The first stage of Phase I, which corresponds to direct Monte Carlo simulation, can be fully scheduled in parallel. In addition, each of the subsequent stages of Phases I and II produces a set of Markov chains that are perfectly parallel. Thus, a number of computer workers can handle the generation of samples corresponding to the different chains [18, 30].

4.6. Final Remarks

Some of the benefits and advantages of using the proposed optimization scheme can be summarized as follows. First, the proposed optimization scheme is based on a well-developed and widely used updating technique (TMCMC method). Thus, the same framework can be adapted for an effective optimization scheme. Second, the methodology produces a set of nearly optimal solutions instead of a single optimal solution. This feature can be advantageous in many practical cases where additional considerations or alternative criteria can be taken into account to select the appropriate final design. Thus, the approach provides flexibility to the decision-making process.

Third, due to the theoretical basis of the approach, it has high chances to reach the vicinity of the global optimum in an effective manner, even in presence of multiple local optima. Fourth, the scheme is a useful tool for exploration of complex feasible design spaces. This is especially useful when design variables exhibit a complex interaction between them. Fifth, the proposed approach provides valuable sensitivity information. In fact, sensitivity of the feasible designs and the final design with respect to the design variables can be obtained directly. Sixth, generally, problems with multiple discontinuous sub-feasible regions can be handled in an effective manner. Seventh, the technique is very-well suited for parallel implementation in a computer cluster. This is extremely important when dealing with optimization problems involving expensive function evaluations such as reliability-based optimization problems. Eight, the proposed constraint-handling technique is direct. Actually, samples in the feasible design space are obtained from the solution of an unconstrained optimization problem which is directly defined in terms of the constraint functions of the original problem. The same framework for obtaining samples in the vicinity of the optimal solution set is used for solving the unconstrained optimization problem. Thus, special constraint-handling techniques are not necessary. This is an advantage from a practical viewpoint. Ninth, due to the generality and flexibility of the formulation, it can handle, in principle, different types of optimization problems. From the structural point of view, these problems may include complex linear and nonlinear systems. Tenth, the proposed framework can handle in a rational and consequent manner problems involving noisy objective or constraint functions (noisy optimization problems), e.g., general performance-based or reliability-based design optimization problems. Finally, the feasibility of solving general constrained optimization problems in the framework of a Bayesian model updating problem provides an additional technique for solving this type of problems.

5. Numerical Examples

It is noted that due to the generality of the proposed approach, a number of optimization problems can be considered as potential examples. As previously pointed out, the focus of this contribution is on the application of the proposed optimization scheme to the reliability-based design optimization of structural dynamical systems under stochastic excitation. Solving this class of problems involves estimating the system reliability at different designs during the optimization process which is well-known to be very challenging from a numerical point of view. In addition, complex physical interactions between the design variables can be obtained, and consequently,

involved feasible design spaces can be generated. Therefore, this is an ideal scenario to evaluate the performance of the proposed optimization scheme. First, two test problems are presented to illustrate the performance of some of the features of the proposed scheme. Specifically, the efficiency of Phase I in relatively complex feasible design spaces is considered. Then, the effectiveness of the optimization algorithm is demonstrated by two application problems involving the reliability-based optimization of structural dynamical systems under stochastic excitation. The following parameter values of the proposed approach are considered for numerical implementation: $\gamma = 0.05$ (stopping criterion parameter); and $\nu = 0.5$ (effective sample size parameter). In addition, the scaling parameter β is determined by an adaptive scheme that monitors the acceptance rate of the updating process with initial value equal to $\beta = 0.1$ [29]. These values have proved to be adequate in the context of this work.

5.1. Test Problem 1

The objective of this test problem is to demonstrate the performance of Phase I in generating samples uniformly distributed over the feasible design space. To focus only on this aspect of the proposed implementation, the optimization problem is defined in terms of analytical functions. The constrained optimization problem takes the form

$$\begin{aligned} \text{Min}_{\mathbf{x}} \;\; & c(\mathbf{x}) \\ \text{s.t.} \;\; & r_i(\mathbf{x}) \leq 1 \;,\; i = 1, ..., 4 \\ & 2.0 \leq x_1 \leq 7.0 \;,\; 0.5 \leq x_2 \leq 5.5 \end{aligned} \tag{18}$$

where $c(\mathbf{x})$ is an arbitrary objective function, and

$$\begin{aligned} r_1(\mathbf{x}) &= 2.0 - \frac{x_1^2 x_2}{20} \\ r_2(\mathbf{x}) &= 2.0 - \frac{93.0}{x_1^2 + 8.0x_2 + 5.0} \\ r_3(\mathbf{x}) &= 2.0 - \frac{(x_1 + x_2 - 10.0)^2}{30.0} - \frac{(x_1 - x_2 + 10.0)^2}{120.0} \\ r_4(\mathbf{x}) &= (0.906x_1 + 0.423x_2 - 6.0)^2 + (0.906x_1 + 0.423x_2 - 6.0)^3 - \\ & 0.6(0.906x_1 + 0.423x_2 - 6.0)^4 - (-0.423x_1 + 0.906x_2) \end{aligned} \tag{19}$$

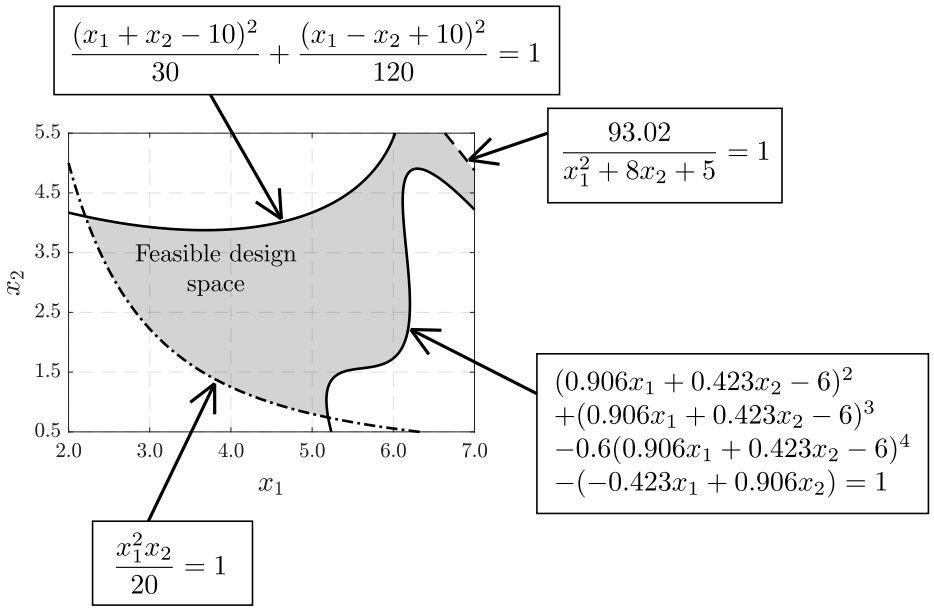

Figure 1: Feasible design space of Test Problem 1.

Figure 1 presents the corresponding feasible design space. The evolution of the samples during the different stages of Phase I is shown in Figure 2. At each stage, 1000 samples are considered for illustration purposes. The number of feasible designs generated at the first three stages are 424, 887 and 1000, respectively. Among them, a total of 980 designs are different. Thus, after three stages, almost 1000 different samples uniformly distributed over the feasible design space are obtained. Such samples are shown in Figure 3. By comparing Figures 1 and 3, it is observed that the samples populate the feasible design space in an effective manner.

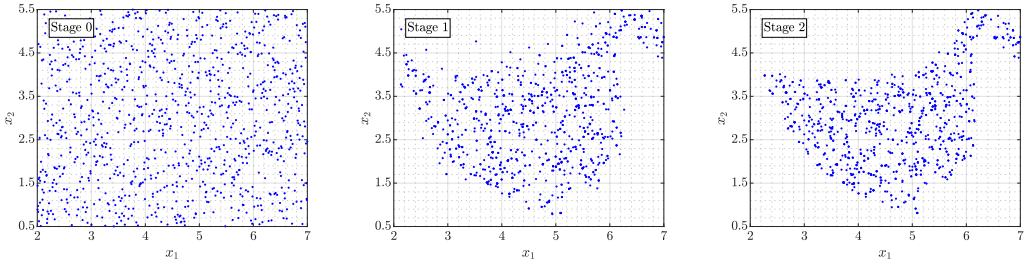

Figure 2: Samples generated at different stages of Phase I. Test Problem 1.

To get more insight into the updating process of Phase I, the marginal conditional distributions of the samples lying in the feasible design space at the final stage of Phase I are shown in Figure 4. The histograms are compatible with the distribution of the samples in the feasible design space, as expected. These samples could be used at the initial stage of Phase II for the purpose of solving the optimization problem formulated in Eq. (18), as previously pointed out.

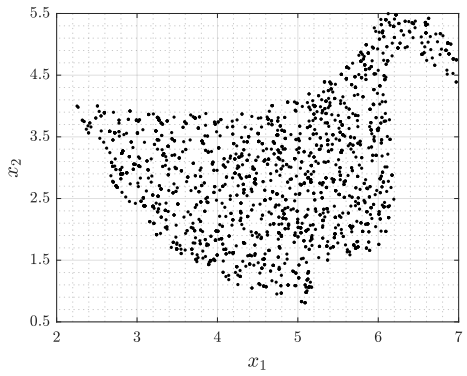

Figure 3: Samples uniformly distributed over the feasible design space. Test Problem 1.

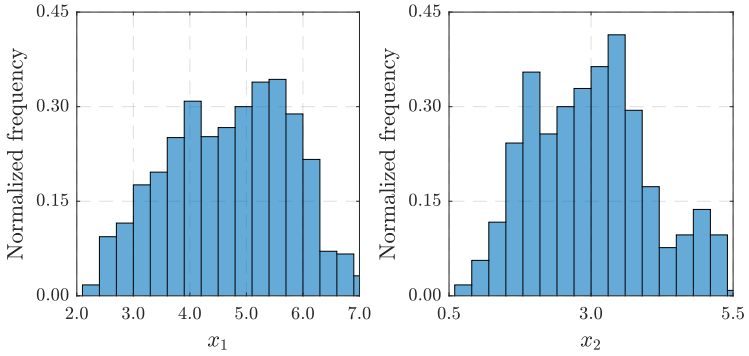

Figure 4: Conditional marginal histograms of the samples obtained at the last stage of Phase I. Test Problem 1.

5.2. Test Problem 2

As in the first test problem, the objective is to illustrate the performance of Phase I. To this end, consider the constrained optimization problem of the form

$$\begin{aligned} \text{Min}_{\mathbf{x}} \quad & c(\mathbf{x}) \\ \text{s.t.} \quad & r(\mathbf{x}) \leq 1 \\ & -3.0 \leq x_1 \leq 3.0 \ , \ -3.0 \leq x_2 \leq 3.0 \end{aligned} \tag{20}$$

where $c(\mathbf{x})$ is an arbitrary objective function, and the constraint function r is given by the so-called six-hump camel-back function, i.e.,

$$r(x_1, x_2) = 1 + 4.0x_1^2 - 2.1x_1^4 + x_1^6/3.0 + x_1x_2 - 4.0x_2^2 + 4.0x_2^4 \tag{21}$$

Figure 5 shows the corresponding feasible design space which is a disconnected region. The evolution of the samples during the different stages of Phase I is shown in Figure 6. One thousand

samples are considered at each stage. After five stages, more than 2000 feasible samples are obtained. Observing the last figure (feasible samples), it is seen that the samples populate the feasible design space in a rather efficient manner.

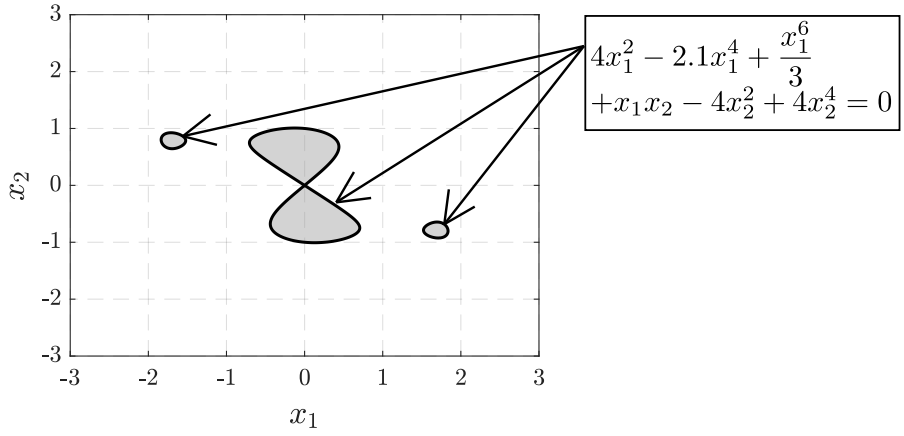

Figure 5: Feasible design space of Test Problem 2. Disconnected region.

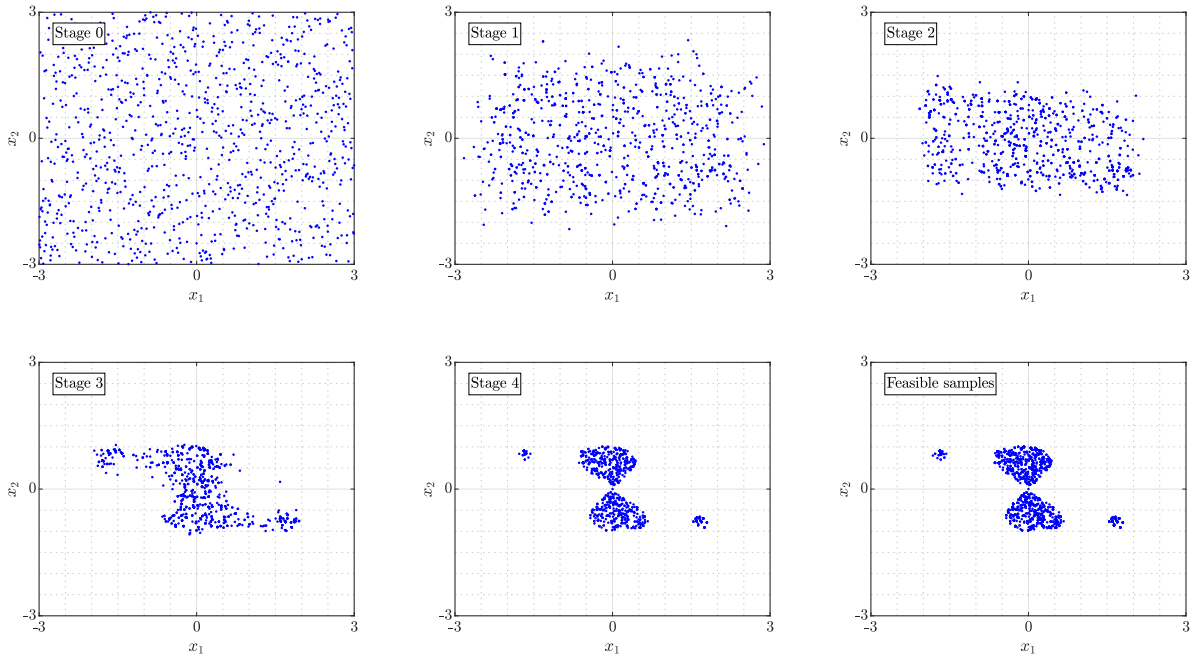

Figure 6: Samples generated at different stages of Phase I. Disconnected region. Test Problem 2.

Another interesting case, where the feasible design space is a region containing interior holes, is given by the problem

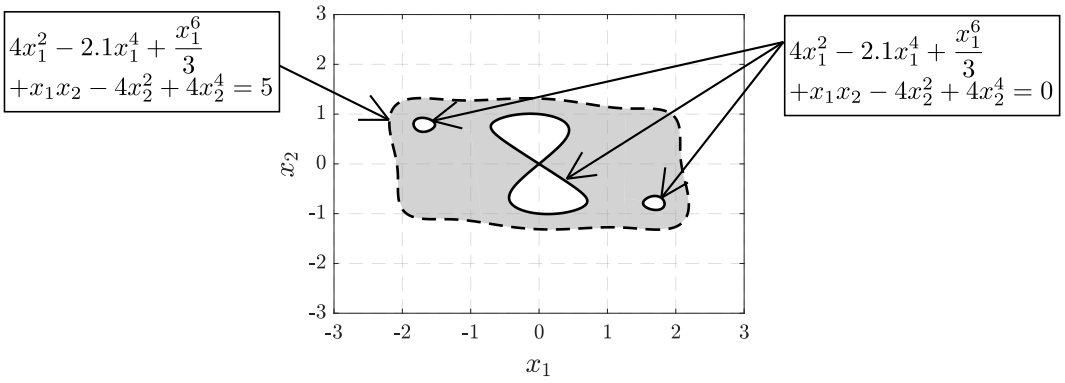

Figure 7: Feasible design space of Test Problem 2. Region with interior holes.

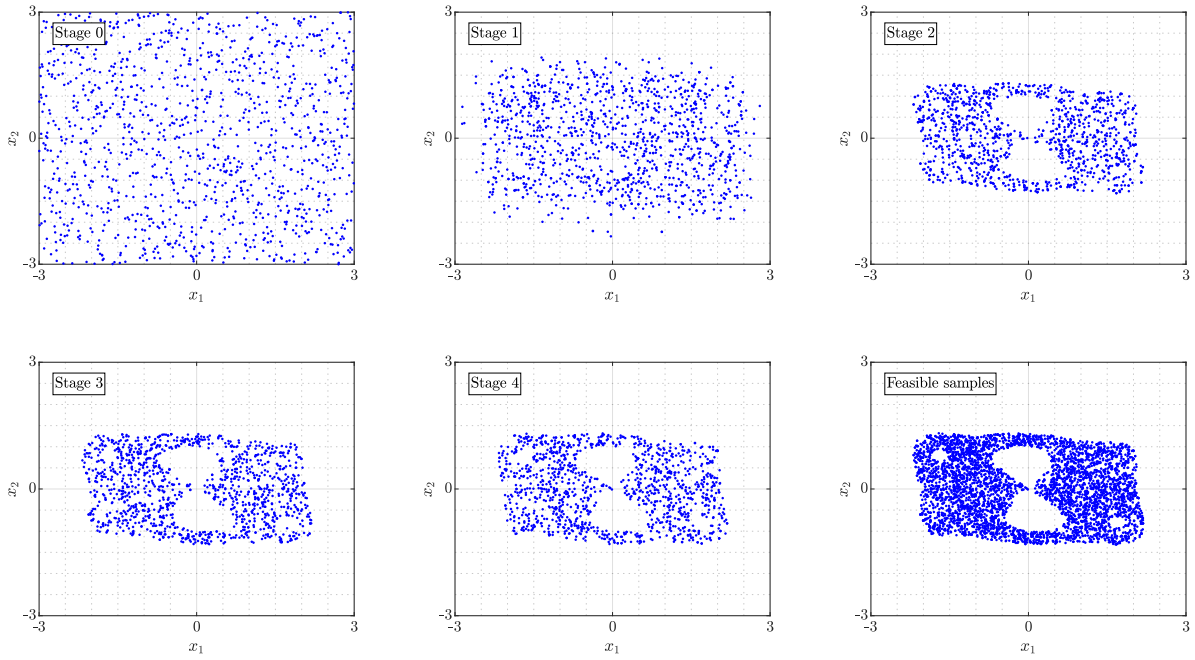

Figure 8: Samples generated at different stages of Phase I. Region with interior holes. Test Problem 2.

$$
\begin{aligned}
\text{Min}_{\mathbf{x}} \quad & c(\mathbf{x}) \\
\text{s.t.} \quad & r_1(\mathbf{x}) \leq 1 \\
& r_2(\mathbf{x}) \leq 1 \\
& -3.0 \leq x_1 \leq 3.0 \ , \ -3.0 \leq x_2 \leq 3.0
\end{aligned} \tag{22}
$$

where $r_1(\mathbf{x}) = 2.0 - r(\mathbf{x})$, and $r_2(\mathbf{x}) = r(\mathbf{x}) - 5.0$. The feasible design space and the evolution of the samples during the different stages of Phase I are shown in Figures 7 and 8, respectively. As in the previous cases, it is clear that the samples occupy the feasible design space in an effective way (see feasible samples figure). The previous results, together with additional validation calculations,

show the effectiveness of Phase I in populating feasible design spaces, even for complex geometries such as disconnected regions and regions containing interior holes. Finally, it is noted that the different quantities involved in the test problems are analytical functions which are inexpensive to evaluate. Thus, the corresponding numerical effort for populating the feasible design spaces is not relevant in the context of these examples.

5.3. Application Problem 1

5.3.1. Model Description

A simple two degree of freedom system subject to stochastic excitation is considered in this application. The model, which is shown in Figure 9, is characterized by normalized masses m_1 and m_2, and normalized stiffnesses k_1 and k_2, which are the parameters to be controlled during the design process. Additionally, 5% of critical damping is added to the model. Though the model is relatively simple from a structural viewpoint, complex interactions between the design variables can be obtained.

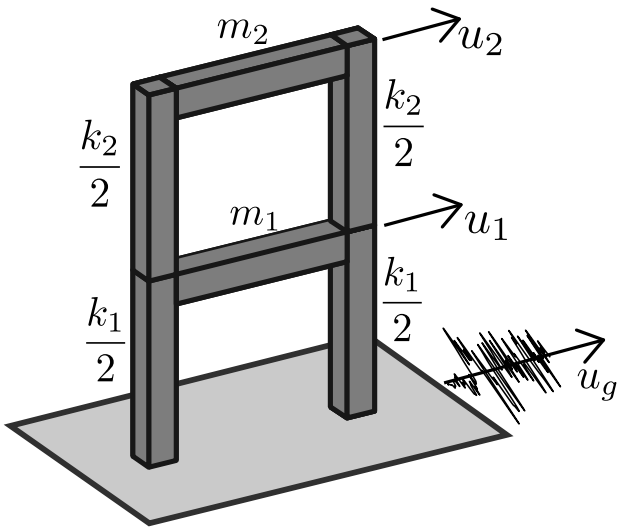

Figure 9: Two-degree-of-freedom system.

The system is subjected to a base acceleration $\ddot{u}_g(t)$, which is modeled as a non-stationary stochastic process. In particular, a stochastic model based on a point-source model is considered [31]. Based on this model, the base acceleration can be expressed as $\ddot{u}_g(t, \mathbf{z})$, where $\mathbf{z} \in \mathbf{Z} \subset R^{n_z}$ is a vector of uncertain parameters involved in the characterization of the excitation. The duration of the excitation is taken as $t_T = 10$s, with a sampling interval equal to $\Delta t = 0.01$s. According to these values, it can be shown that the generation of ground motion samples comprises more

than 1000 random variables [31, 32]. A detailed description and implementation of the stochastic excitation model can be found in [31, 33, 34]

5.3.2. Optimization Problem

The design problem is written in the form

$$\begin{aligned} \text{Min}_{\mathbf{x}} \quad & c(\mathbf{x}) \\ \text{s.t.} \quad & x_2/x_1 \leq 1 \\ & P_F(\mathbf{x})/10^{-2} \leq 1 \\ & 1.0 \leq x_i \leq 5.0 \ , \ i = 1, 2 \end{aligned} \tag{23}$$

where $x_i, i = 1, 2$ are the design variables, that is, $x_1 = k_1$ and $x_2 = k_2$, and $P_F(\mathbf{x})$ is the system failure probability evaluated at the design $\mathbf{x}$. For illustration purposes, the objective function is assumed to be proportional to the stiffnesses k_1 and k_2. In particular, $c(\mathbf{x}) = (x_1 + x_2)/10$. The failure probability $P_F(\mathbf{x})$ is defined in terms of a failure event associated with the interstory drifts and the total accelerations at the first and second floor. The characterization of the failure event and the corresponding reliability problem is provided in Appendix A. It is noted that the estimation of the probability of failure for a given design, i.e., $P_F(\mathbf{x})$, constitutes a high-dimensional problem which is extremely demanding from a numerical point of view. Such quantity is usually estimated by advanced simulation techniques [32, 40, 41].

5.3.3. Results

The related iso-probability curves are shown in Figure 10. These curves are constructed by using a set of failure probability estimates distributed over the design space. The estimates are obtained by Subset simulation [32]. The resulting curves, which are rather rugged because of the variability of the probability estimates, have been smoothed for presentation purposes. The corresponding feasible design space is sketched in Figure 11, where some contour curves of the objective function are also shown as well as the optimal design. Due to the responses involved in the definition of the failure event, a highly complex interaction between the design variables is observed.

The evolution of the samples during the different stages of Phase I is shown in Figure 12. At each stage, 500 samples are considered for illustration purposes. After three stages, more than

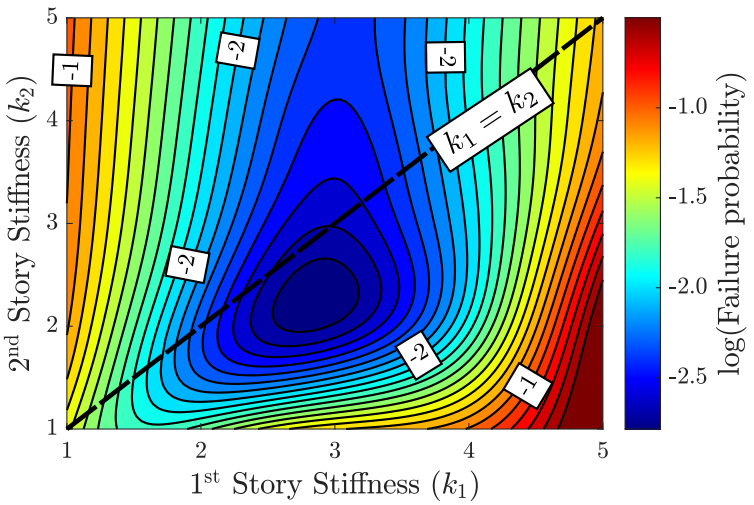

Figure 10: Iso-probability curves. Application Problem 1.

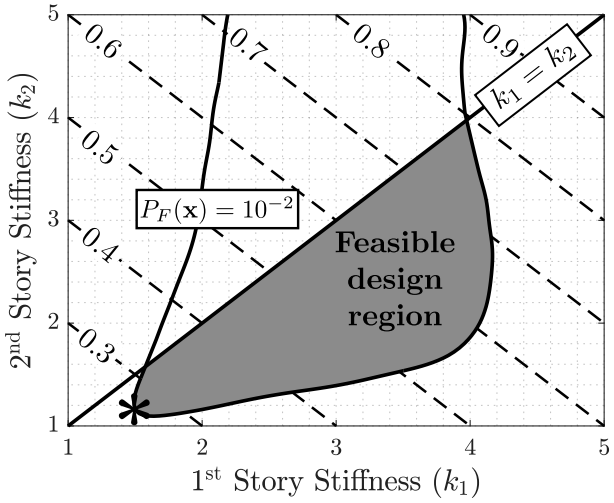

Figure 11: Sketch of the feasible design space, some contour curves of the objective function, and optimal design ($*$). Application Problem 1.

500 different feasible designs are generated. These samples, which are uniformly distributed over the feasible design space, are shown in Figure 13. Note that the shape generated by these samples shows an excellent agreement with the feasible design space shown in Figure 11.

Next, the minimization problem formulated in Eq. (23) is solved by the proposed Phase II, where the number of samples per stage is set equal to 500. The samples obtained from the first five stages are shown in Figure 14. At the last stage, the samples populate a vicinity of the optimal solution set, which is consistent with Figure 11. The range of the objective function values obtained during the different stages is shown in Figure 15. The minimum value obtained during the simulation process (sample-based optimum cost) is equal to 0.25, which is associated with the

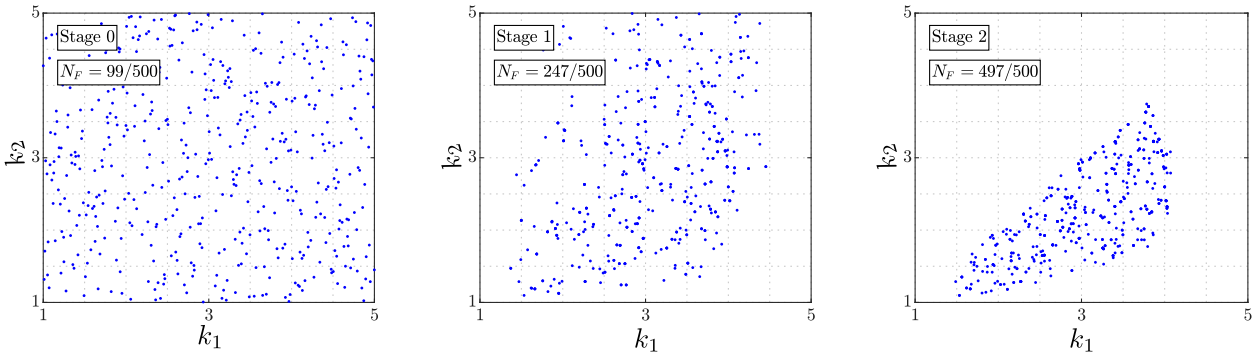

Figure 12: Evolution of samples generated at different stages of Phase I. Application Problem 1.

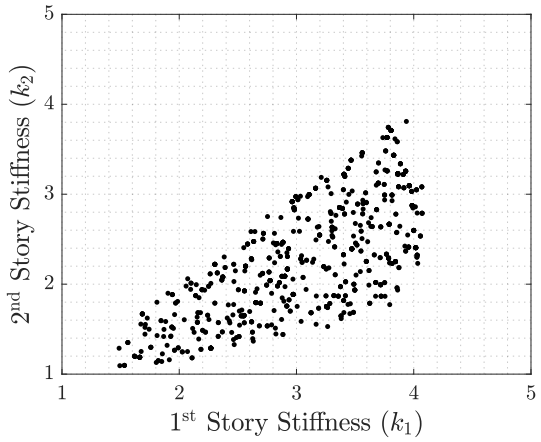

Figure 13: Samples uniformly distributed over the feasible design space. Application Problem 1.

design $k_1 = 1.43$ and $k_2 = 1.10$, and corresponding reliability constraint value $P_F/10^{-2} = 0.96$, and geometric constraint $x_2/x_1 = 0.74$. Considering the variability involved in the estimation of the probability of failure, the reliability constraint can be considered as active at the final design. Note that this result is compatible with the information provided by Figure 11.

Finally, observing Figure 15, it is seen that the minimum value of the objective function at Stage 0 of Phase II, i.e., at the designs uniformly distributed over the feasible design space, is relatively close to the sample-based optimal cost, i.e., minimum value of the objective function at Stage 5. Thus, the best solution among the samples generated during Phase I gives a good approximation for the value of the objective function at the final design in this case. It is noted that however, Phase II can provide valuable information about the sensitivity of the final design with respect to the design variables in the vicinity of the final design. This information is quite relevant, specially when dealing with several design variables and complex feasible design spaces.

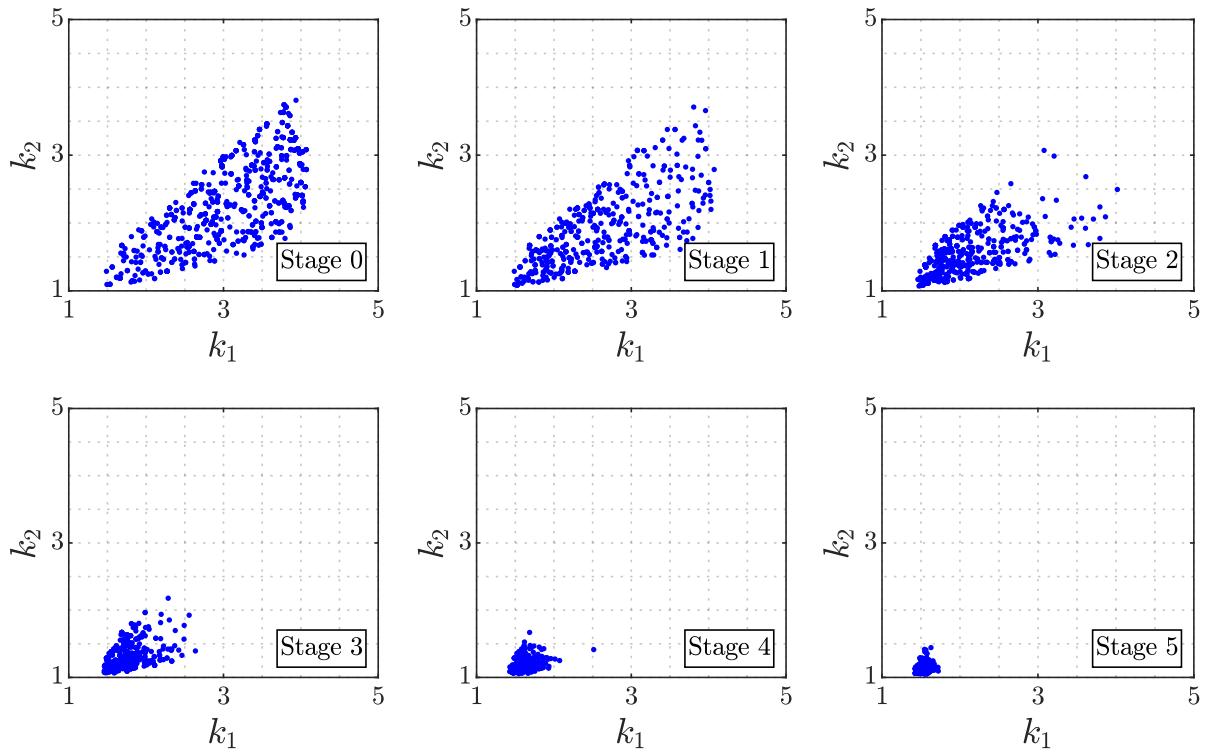

Figure 14: Evolution of samples generated at different stages of Phase II. Application Problem 1.

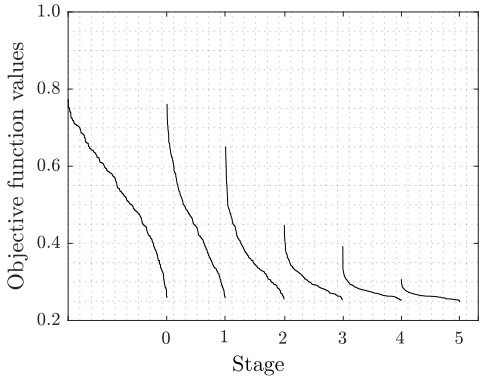

Figure 15: Objective function values at different stages of Phase II. Application Problem 1.

5.3.4. Numerical Effort and Comparison

Considering that the total number of sampling stages involved in the optimization process is equal to 8, and that 500 samples are used per stage, the total number of function evaluations is equal to 4000. In this regard, it is noted that a study about the statistical performance of the proposed design scheme in this example problem indicates that the scheme performs in an effective manner even when the number of samples per stage is much smaller than 500. Recall that this number was used only for illustration purposes, as previously pointed out. In other words, the algorithm is capable to obtain the optimal solution set in an effective manner with a

relatively small number of samples per stage. Thus, the number of function evaluations (reliability estimates) indicated before overestimates the actually required number.

The comparison of the performance of the proposed optimization scheme with respect to some alternative methods is provided in Table 1. In particular, the following stochastic optimization algorithms are considered: genetic algorithm based on dominance-based tournament selection (GAS) [8]; subset simulation-based optimization (SSBO) [14]; co-evolutionary particle swarm optimization (CPSO) [35]; hybrid particle swarm optimization with a feasibility-based rule (HYPSOR) [36]; genetic algorithm based on a co-evolution model (GAC) [37]; and harmony search (HS) [38]. The second column of the table corresponds to the function-call factor which is the ratio of the number of function evaluations involved in a given algorithm and the number of function evaluations involved in the proposed scheme. The algorithms were calibrated, in terms of the number of function calls, in such a way that similar final designs were obtained.

Algorithm	Function-call factor
GAS	6.1
SSBO	6.2
CPSO	14.1
HYPSOR	6.1
GAC	64.1
HS	6.1
Proposed	1.00

Table 1: Comparison of numerical efforts with respect to alternative algorithms.

It is seen that the proposed algorithm compares very favorably with respect to the other population-based stochastic optimization algorithms for this example problem. The algorithm needs the least number of reliability analyses to solve the problem. In fact, the proposed scheme requires less than one sixth of the function calls involved in the other methods.

5.4. Application Problem 2

5.4.1. Structural Model

A finite element model with about 50000 degrees of freedom is analyzed in the second application problem. The model consists of a non-linear 52-story building under stochastic earthquake

excitation. An isometric view of the structural system is shown in Fig. 16. The plan view and the dimensions of each floor are shown in Fig. 17. The inter-story height is 3.6 m for all floors except the first one which has a height of 14 m.

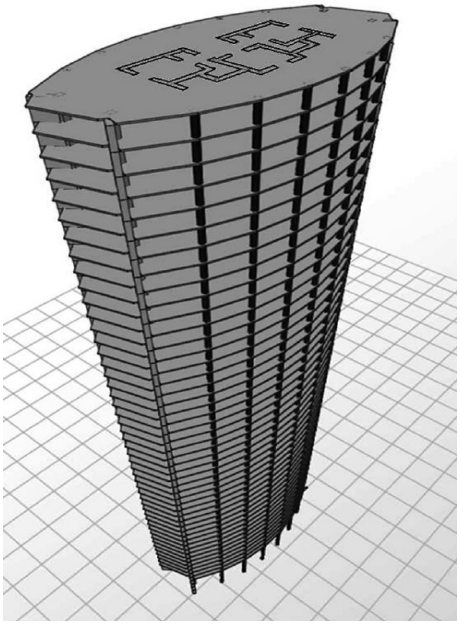

Figure 16: Isometric view of the 52-story building model

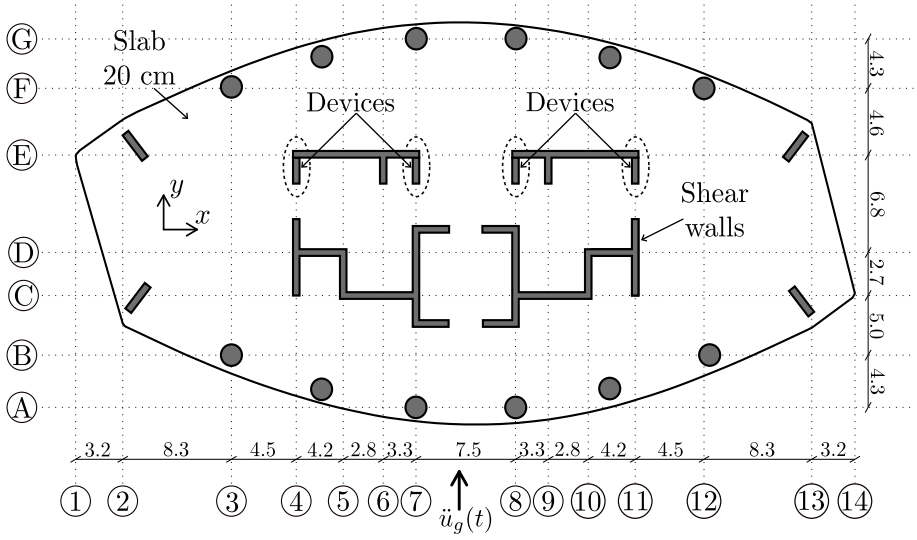

Figure 17: Floor plan of the 52-story building model

The building has a reinforced concrete core of shear walls and a reinforced concrete perimeter moment frame as shown in Fig. 17. The columns in the perimeter have a circular cross section.

The nominal value for the column's diameter and shear wall's thickness is 0.40 m. In addition, the slab thickness is equal to 0.20 m. Properties of the reinforced concrete have been assumed as follows: Young's modulus $E = 2.45 \times 10^{10}$ N/m^2, Poisson's ratio $\mu = 0.3$, and mass density $\rho = 2500$ kg/m^3. For the dynamic analysis, it is assumed that each floor may be represented as rigid within the plane when compared with the flexibility of the other structural components. Then, the degrees of freedom of the finite element model are linked to three degrees of freedom per floor (two translational displacements and one rotational displacement) by using condensation techniques. A 5% of critical damping for the modal damping ratios is introduced in the model. The building is excited horizontally by a ground acceleration $\ddot{u}_g(t)$ in the y direction as shown in Fig 17. The excitation is modeled as in the previous example problem. The sampling interval is assumed to be $\Delta t = 0.01$s, and the duration of the excitation is $t_T = 15$s.

For aseismic design purposes, the model is reinforced with nonlinear hysteretic devices. At each floor, four devices are implemented as shown on the floor plan of the structure (axes 4, 7, 8, and 11). These elements provide additional resistance and dissipation against relative displacements between floors. Each non-linear device follows the interstory restoring force law $r(t) = k^e(\delta u(t) - q_1(t) + q_2(t))$, where k^e denotes the initial stiffness of the non-linear device, $\delta u(t)$ is the relative displacement between floors at the position of the device in the y direction, and $q_1(t)$ and $q_2(t)$ denote the plastic deformations of the device. The restoring force $r(t)$ acts between adjacent floors with the same orientation as the relative displacement $\delta u(t)$. Using the auxiliary variable $v(t) = \delta u(t) - q_1(t) + q_2(t)$, the plastic elongations are specified by the first-order nonlinear differential equations [39]

$$\dot{q}_i(t) = (-1)^{i+1}\dot{\delta}u(t)H\Big((-1)^{i+1}\dot{\delta}u(t)\Big)\Big[H\Big((-1)^{i+1}v(t) - v_y\Big)\frac{(-1)^{i+1}v(t) - v_y}{v_p - v_y}$$
$$H\Big(v_p - (-1)^{i+1}v(t)\Big) + H\Big((-1)^{i+1}v(t) - v_p\Big)\Big]\ ,\ i = 1, 2 \tag{24}$$

where $H(\cdot)$ denotes the Heaviside step function, $\dot{\delta}u(t)$ is the relative velocity between floors at the position of the device in the y direction, v_y is a parameter specifying the onset of yielding, and $k^e v_p$ is the maximum restoring force of the device. All devices have initial stiffness $k^e = 2.8 \times 10^9$ N/m, and model parameters $v_p = 0.006$ m and $v_y = 0.0042$ m. Note that the evaluation of the system response involves the solution of a system of coupled differential equations, that is, the equation of motion of the structural system and the equation for the evolution of the variables describing

the plastic deformation of the non-linear devices. The equations are solved by an appropriate step-by-step integration scheme.

5.4.2. Design Problem

The variables to be controlled are the thicknesses of the concrete core of shear walls (t_w) and the diameters of the exterior columns (d_c). The dimensions of these structural components at each floor are linked to one intermediate optimization variable, x, as $t_w = x\ \hat{t}_w$, and $d_c = x\ \hat{d}_c$, where $\hat{t}_w$ and $\hat{d}_c$ are the nominal values of the thickness of the shear walls and the diameter of the exterior columns at each floor, respectively. The intermediate optimization variables are grouped into a number (n_d) of optimization variables. The objective function for the design problem is defined in terms of the intermediate optimization variables. Two reliability constraints are considered in the present example. The constrained optimization problem is formulated as

$$\begin{aligned} &\text{Min}_{\mathbf{x}} \quad c(\mathbf{x}) \\ &\text{s.t.} \quad P_{F_1}(\mathbf{x})/10^{-3} \leq 1 \ \ , \ \ P_{F_2}(\mathbf{x})/10^{-3} \leq 1 \\ &\qquad x_{i+1}/x_i \leq 1 \ \ , i = 1, 2, ..., n_d - 1 \quad , \ \ 0.5 \leq x_i \leq 1.50 \ , \ i = 1, 2, ..., n_d \end{aligned} \tag{25}$$

where the failure probability $P_{F_1}(\mathbf{x})$ is defined in terms of a failure event associated with the interstory drift of the first floor, and $P_{F_2}(\mathbf{x})$ is given in terms of a failure event related to the roof displacement. The characterization of the failure events is provided in Appendix B. Similarly to the first application problem, the estimation of the probability of failure for a given design requires considerable numerical efforts.

5.4.3. Use of Meta-Model

It is noted that the proposed Two-Phase approach may require a large number of reliability analyses for populating the region containing the optimal solution set. Clearly, the failure probabilities at the different designs can be estimated directly during the design process, as in the previous example. However, the numerical demands may become excessive when the computational time for estimating the failure probability functions is significant. To deal with this issue, an adaptive kriging-based meta-model for approximating the failure probability functions is considered in the present example. Information about the meta-model is given in Appendix C.

5.4.4. Results: First Scenario

In this scenario, two design variables are considered. The first design variable is associated with the lower 26 floors, while the second design variable corresponds to the upper 26 floors of the building. The reliability-based optimal design problem is written in terms of a normalized objective function as

$$\begin{aligned} \text{Min}_{\mathbf{x}} \;\; & c(\mathbf{x}) \\ \text{s.t.} \;\; & P_{F_1}(\mathbf{x})/10^{-3} \leq 1 \;\; , \;\; P_{F_2}(\mathbf{x})/10^{-3} \leq 1 \\ & x_2/x_1 \leq 1 \;\; , \;\; 0.5 \leq x_i \leq 1.5 \;\; , \; i = 1, 2 \end{aligned} \tag{26}$$

where $c(\mathbf{x}) = \sum_{i=1}^{2} x_i$. Figure 18 shows some iso-probability curves and the corresponding sketch of the feasible design space, including the optimal design. As in the previous example, the curves have been smoothed for presentation purposes. It is observed that the iso-probability curves associated with the interstory drift of the first floor (continuous-lines) show a rather weak interaction between the design variables. In fact, the curves present an important dependence on the design variable related to the thickness of the shear walls and the diameter of the exterior columns at the lower floors (x_1). On the other hand, the iso-probability curves related to the roof displacement (dashed-lines) show a strong interaction between both design variables, as expected. Note that these results give a valuable insight into the interaction and effect of the design variables on the reliability of this complex system.

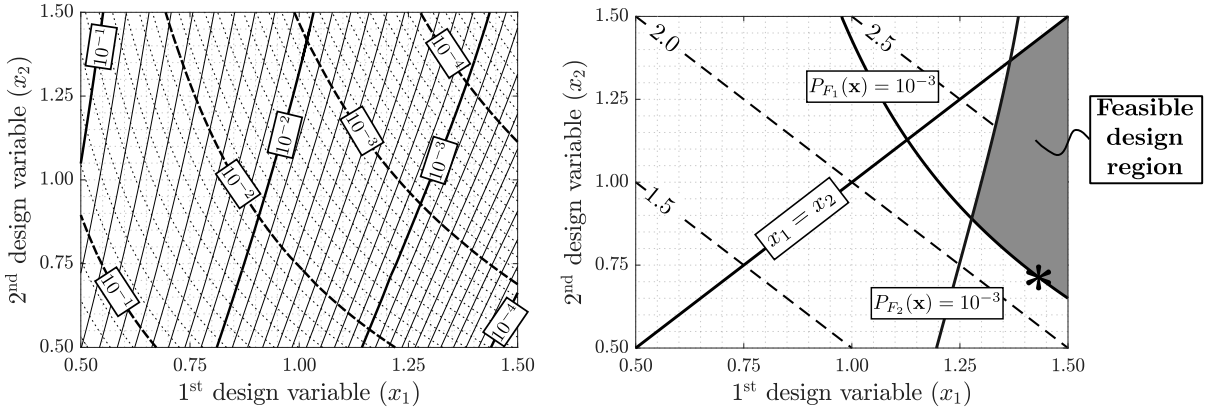

Figure 18: Left figure: Iso-probability curves. P_{F_1}: continuous lines, P_{F_2}: dashed-lines. Right figure: sketch of the feasible design space with the optimal design (asterisk). Application Problem 2. First scenario.

The set of feasible samples uniformly distributed over the feasible design space is shown in

Figure 19 (Stage 0). This information correspond to all feasible designs obtained during Phase I. For illustration purposes, the algorithm is implemented by considering 500 samples per stage. There are about 500 samples of which more than 200 are different after three stages. The shape generated by these samples agrees very well with the feasible design space shown in Figure 18 (right figure). The designs obtained from the first five stages of Phase II are also shown in Figure 19. At the last stage, the values of the normalized objective function range from 2.121 to 2.140. The associated optimal design is given by $x_1 = 1.413$ and $x_2 = 0.708$, with corresponding reliability constraint values $P_{F_1}/10^{-3} = 0.999$, and $P_{F_2}/10^{-3} = 0.218$. Thus, the reliability constraint associated with the interstory displacement of the first floor is active at the final design, which is consistent with Figure 18 (right figure).

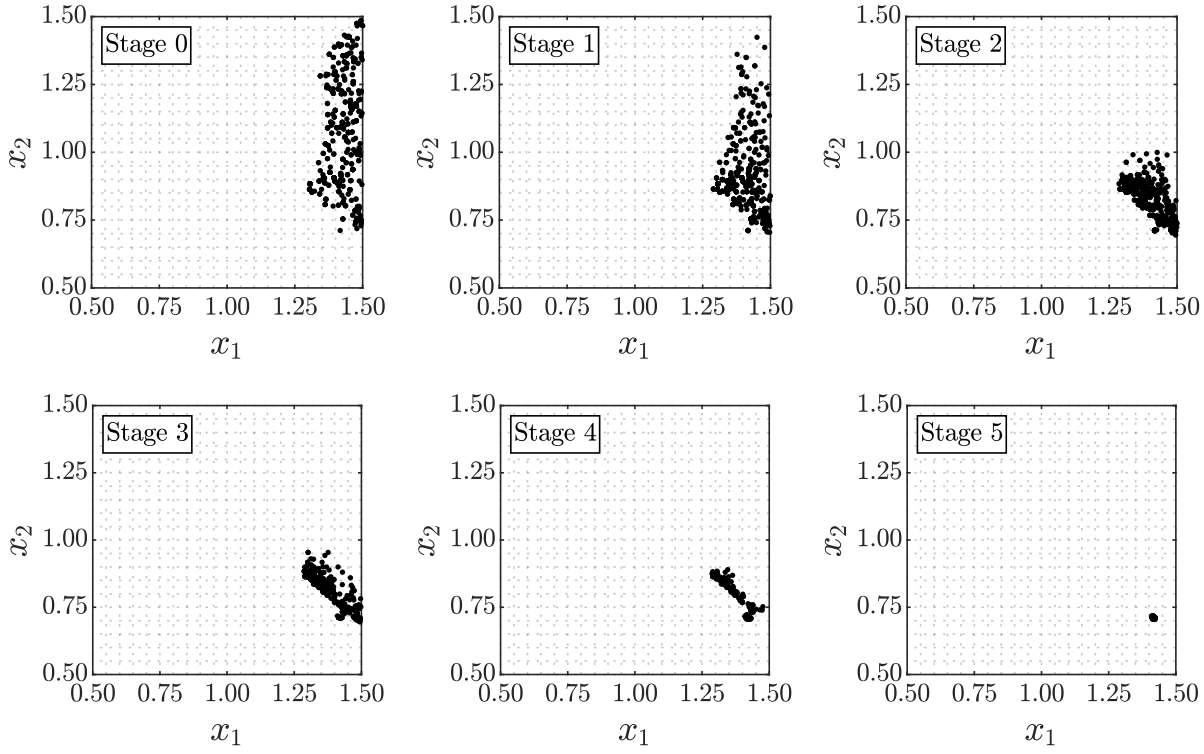

Figure 19: Feasible samples (Stage 0), and the evolution of samples generated at different stages of Phase II. Application Problem 2. First scenario.

Information about the use of kriging during the different stages of Phase II is shown in Figure 20. The number of support points is equal to 12 and an error tolerance level $\epsilon = 0.1$ is selected (see Appendix C). These values proved to be adequate for the current optimization problem. Once the initial database of support points has been constructed, the surrogate acceptance ratio is almost 100%. Thus, almost all surrogate estimates are accepted from the second stage of Phase II. In this

context, the acceptance ratio represents the fraction of failure probability evaluations obtained with the kriging approximation. Overall, that is, considering the generation of the database, more than 87% of the total number of reliability evaluations are performed using the meta-model. The previous level of acceptance ratio clearly indicates the efficiency of the proposed adaptive meta-model scheme. This high level of acceptance ratio is due to the fact that the failure probability functions involved in the problem are smoothly varying with respect to the design variables, and thus the surrogate estimates are quite accurate for most of the samples. In terms of accuracy, validation calculations show that the previous results are very similar to those obtained when the reliability constraints are estimated directly, that is, when the meta-model is not used. In fact, the sample-based normalized optimum cost obtained by the proposed approach, i.e., 2.121, is only 0.07% higher than the one obtained without using the kriging approximation. In relation to the computational cost, a speedup close to 10 is obtained by the proposed approach. In this context, the speedup is the ratio of the execution time by solving the design problem directly and the execution time by using the proposed approximation of the failure probabilities during the design process. The actual total number of function evaluations during the entire optimization process is around 500. This small number of function evaluations indicates that use of the proposed meta-model for approximating the reliability constraints is quite beneficial in terms of computational efficiency.

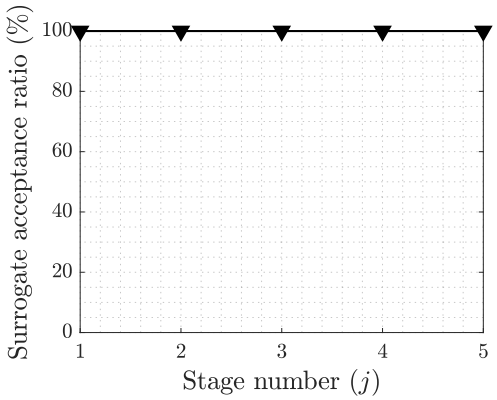

Figure 20: Use of kriging during the different stages of Phase II. Application Problem 2. First scenario.

5.4.5. Results: Second Scenario

Under this scenario, the intermediate design variables are grouped into six optimization variables. The definition of these variables is given in Table 2.

Design variable	x_1	x_2	x_3	x_4	x_5	x_6
Design elements (floors)	$1-9$	$10-18$	$19-26$	$27-35$	$36-44$	$45-52$

Table 2: Linking detail of intermediate optimization variables

The reliability-based design optimization problem takes the form

$$\begin{aligned} \text{Min}_{\mathbf{x}} \;\; & c(\mathbf{x}) \\ \text{s.t.} \;\; & P_{F_1}(\mathbf{x})/10^{-3} \leq 1 \;\; , \;\; P_{F_2}(\mathbf{x})/10^{-3} \leq 1 \\ & x_{i+1}/x_i \leq 1 \;\; , i = 1, 2, ..., 5 \quad , \;\; 0.5 \leq x_i \leq 1.5 \;\; , \; i = 1, 2, ..., 6 \end{aligned} \tag{27}$$

where $c(\mathbf{x}) = \sum_{i=1}^{6} x_i$, and the failure events are the ones defined in the first scenario. As in the previous case, the algorithm is implemented by considering 500 samples per stage. The feasible samples obtained after eight stages of Phase I are shown in Figure 21. This figure shows the two-dimensional projections and marginal distributions of the feasible designs obtained after eight steps. A total of 950 feasible samples are obtained, among which 275 are distinct. It is noted that the volume of the feasible design space is very small with respect to the initial design space. In fact, the volume ratio is about 0.01% according to preliminary validation calculations. Then, it is seen that the approach is capable of obtaining samples from the feasible design space even in challenging geometries as in this case.

The set of samples obtained after ten stages of Phase II are shown in Figure 22. It is observed that the samples are concentrated near a single value. At the last stage, the values of the normalized objective function range from 6.333 to 6.357. Then, the minimum value (sample-based optimal cost) is equal to 6.333, which is associated with the design $\mathbf{x}^T =< 1.489, 1.476, 1.088, 1.011, 0.751, 0.515 >$. The corresponding reliability constraint values are $P_{F_1}/10^{-3} = 0.999$, and $P_{F_2}/10^{-3} = 0.169$. Thus, the reliability constraint associated with the interstory displacement of the first floor is active at the final design, which is compatible with the first scenario. On the other hand, the geometric constraint values are: $x_2/x_1 = 0.991$; $x_3/x_2 = 0.736$; $x_4/x_3 = 0.930$; $x_5/x_4 = 0.743$; and $x_6/x_5 = 0.685$. Based on these results, the first geometric constraint can be considered as active at the final design. It is seen that the final design favors large values of the optimization variables associated with the columns's diameter and shear wall's thickness of the lower floors, which is consistent from the structural point of view. Note that the same feature is exhibited by the final

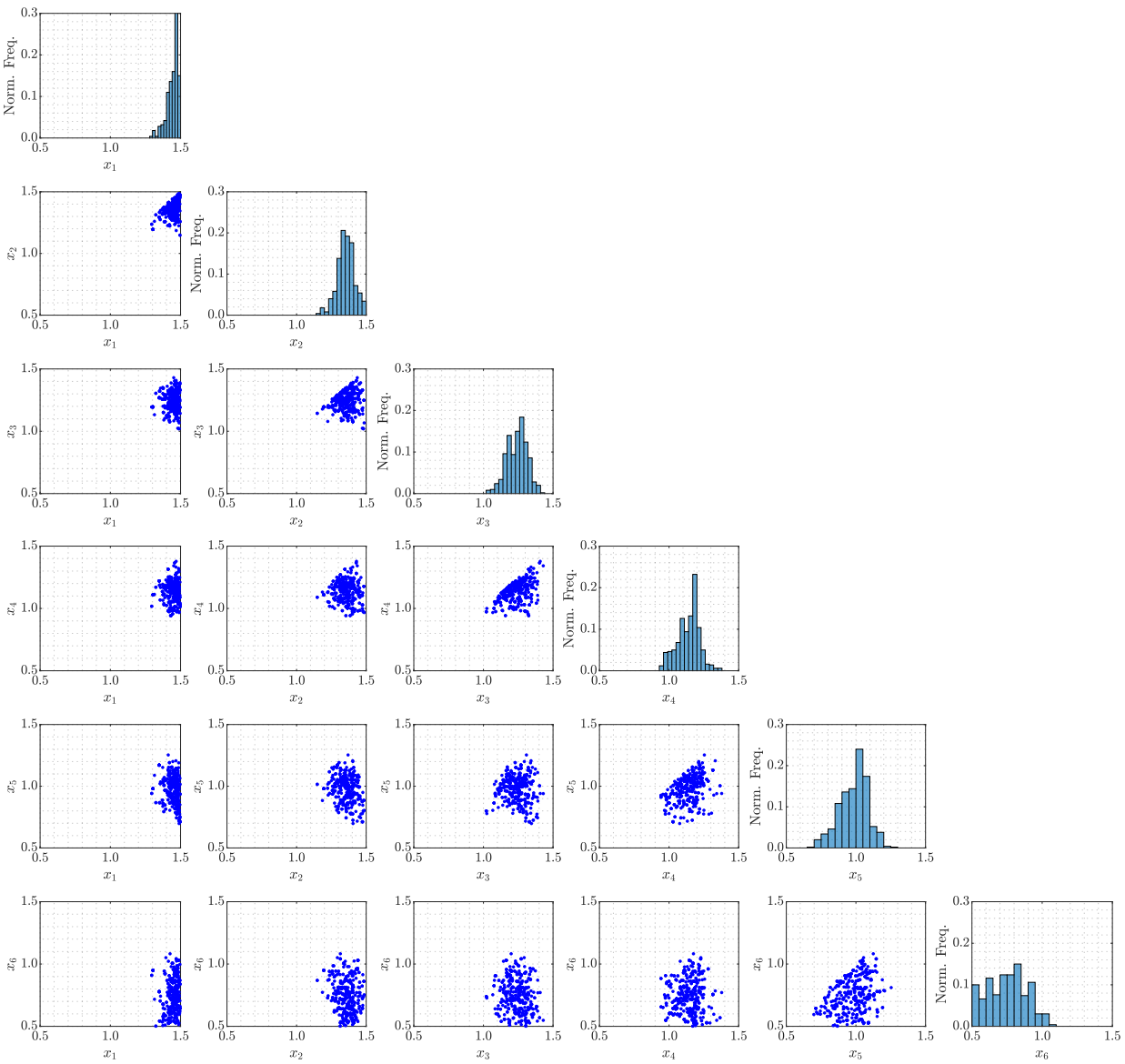

Figure 21: Two-dimensional sample projections and marginal histograms of feasible samples obtained at the last stage of Phase I. Application Problem 2. Second scenario.

design obtained when considering only two design variables (first scenario). Thus, the final designs obtained from both scenarios are qualitatively similar. However, note that the distribution of the stiffness over the height of the building is more regular in the present scenario, which is reasonable from the optimization point of view (six control or optimization variables instead of two).

The evolution of the surrogate acceptance ratio during the design process is shown in Figure 23. In particular, this figure shows the acceptance ratio during Phase II. The number of support points in the context of kriging approximations is equal to 28. This number proved to be adequate for the current scenario. The acceptance rate remains very high during the entire process. Actually,

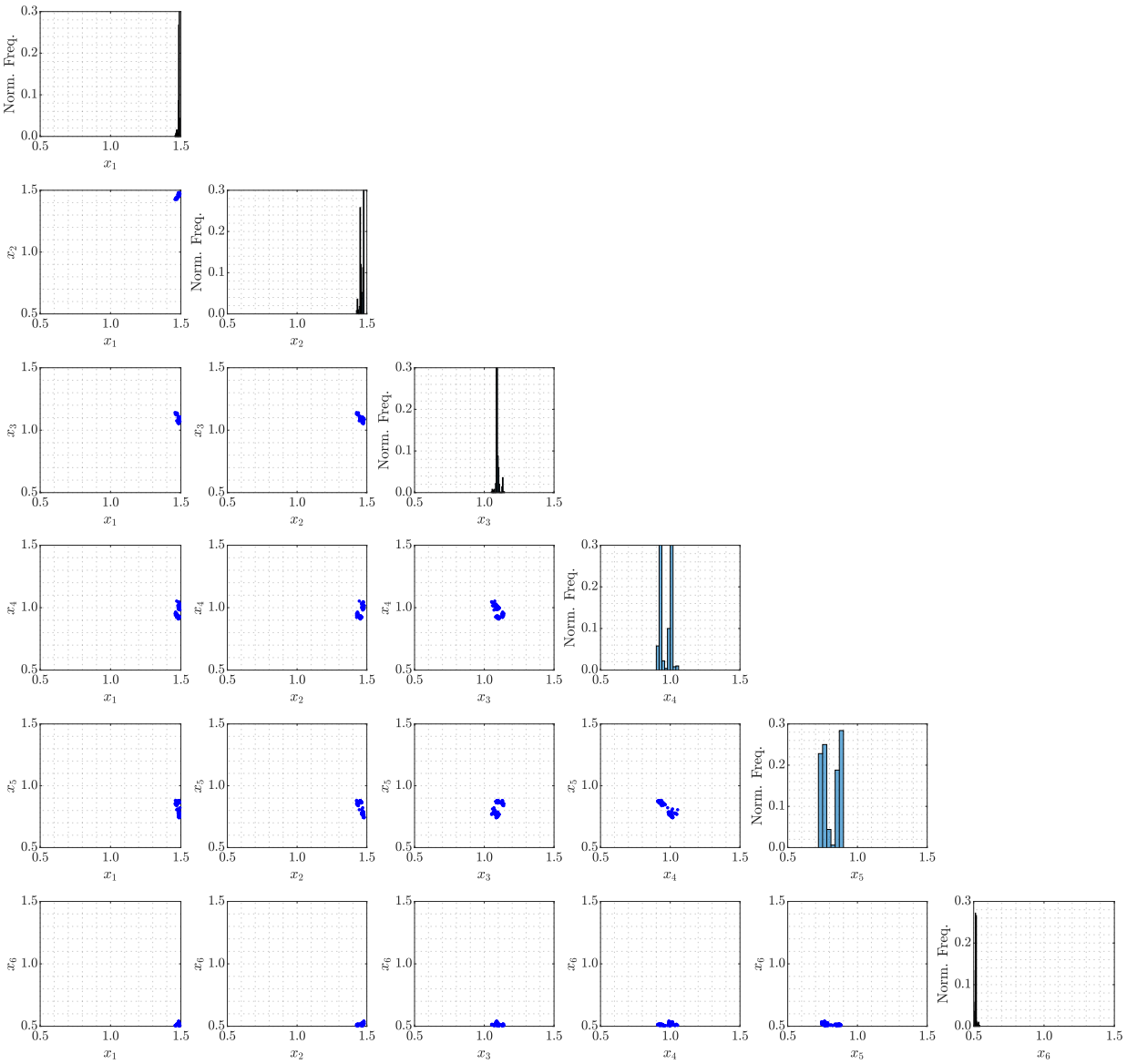

Figure 22: Two-dimensional sample projections and marginal histograms of the design variables obtained at the last stage of Phase II. Application Problem 2. Second scenario.

the number of reliability estimates that need to be evaluated directly is less than 6% of the total number of estimates required during the entire optimization process (Phases I and II). Thus, the efficiency of the proposed adaptive scheme is also evident in the context of this scenario. As in the first scenario, the failure probability functions involved in the problem are smoothly varying with respect to the design variables, and thus the surrogate estimates are quite accurate for most of the samples. Validation calculations show that the previous results are very similar to those obtained when the reliability constraints are estimated directly.

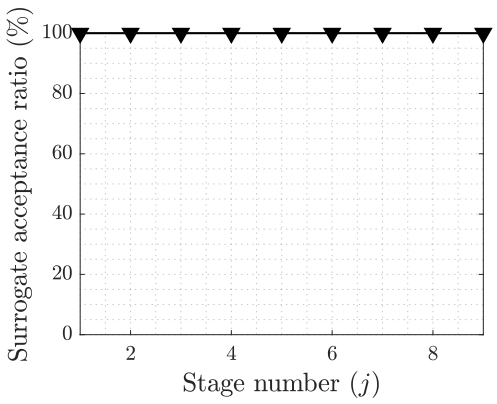

Figure 23: Use of kriging during the different stages of Phase II. Application Problem 2. Second scenario.

5.4.6. Computational Effort

The corresponding speedup factor obtained by the proposed scheme is more than 16 in this case, and the total number of function evaluations (reliability analyses) during the entire optimization process is close to 500. This small number of function calls indicates that the use of the proposed meta-model is very advantageous in terms of computational cost. Note that this significant reduction in computational effort is obtained without compromising the accuracy of the design process. To make a fair comparison of the proposed optimization scheme with other population-based stochastic optimization algorithms it is necessary to develop meta-models in the framework of those algorithms. Clearly, this is beyond the scope of the present contribution. Finally, the results of this application problem show that the use of surrogate modeling techniques together with the proposed optimization scheme can be an efficient and practical choice for solving the class of complex problems considered in the present work.

6. Conclusions

A population-based stochastic optimization scheme for solving general constrained optimization problems has been presented. The problem is set into a framework of a Two-Phase Bayesian model updating problem. Phase I generates designs uniformly distributed over the feasible design space, while Phase II obtains a set of designs lying in the vicinity of the optimal solution set. The model updating problem is solved by the transitional Markov chain Monte Carlo method. The proposed constraint-handling approach is direct and does not require special constraint-handling techniques. Actually, the same framework for obtaining samples in the vicinity of the optimal solution set is used for obtaining samples in the feasible design space. In addition, the scheme

produces a set of nearly optimal solutions instead of a single optimal solution. This feature can be advantageous in many practical cases, where additional considerations or alternative criteria can be taken into account to select the appropriate final design. Thus, the approach provides flexibility to the decision-making process. Moreover, due to the generality and flexibility of the formulation, it can handle different types of structural optimization problems involving linear and nonlinear models.

The general approach is applied to an important class of problems. Specifically, reliability-based design optimization of structural dynamical systems under stochastic excitation. The results of the example problems indicate that the samples generated by Phase I populate the feasible design space in an effective manner, even in problems involving challenging geometries. Thus, the proposed scheme is a useful tool for exploration of complex feasible design spaces. Moreover, at the last stage of Phase II, the samples are distributed in the vicinity of the optimal solution set. In terms of computational efficiency, the results indicate that the proposed algorithm compares favorably with respect to other population-based stochastic optimization algorithms.

When dealing with complex reliability-based design optimization problems, the use of meta-models can be very attractive. In fact, the numerical results of application 2 show that high surrogate acceptance rates are obtained during the entire design process. In this manner, a small percentage of direct reliability estimations is required during the procedure allowing substantial savings in computational efforts. Beside, the reduction in computational effort is obtained without compromising the accuracy of the design process. Thus, the use of surrogate modeling techniques together with the proposed optimization scheme may provide an effective numerical tool for dealing with the stochastic optimization of complex structural models.

A future research effort aims to implement the proposed approach to more complex and involved stochastic structural optimization problems. In these cases, the proposed optimization scheme can be combined with parametric reduced-order models. The idea is to perform structural analyses in terms of reduced-order models instead of full finite element models. The extension of the methodology to stochastic optimization problems involving mixed-design variables is an additional topic for future research. Work in these directions is currently under way.

Acknowledgments

The research reported here was supported in part by CONICYT (National Commission for Scientific and Technological Research) under grant number 1200087. Also, this research has been supported by CONICYT and DAAD under CONICYT-PFCHA/Doctorado Acuerdo Bilateral DAAD Becas Chile/2018-62180007. In addition, this research has been implemented under the PAC (Programa Asistente Cientifico 2017)-UTFSM program. These supports are gratefully acknowledged by the authors.

7. Appendix A

The failure event F is characterized as $F(\mathbf{x}, \mathbf{z}) = d(\mathbf{x}, \mathbf{z}) > 1$, where d is a demand function given by

$$d(\mathbf{x}, \mathbf{z}) = \max_{j=1,2} \max_{t \in [0, t_T]} \left\{ \frac{|\delta u_j(t, \mathbf{x}, \mathbf{z})|}{\delta^*}, \frac{|a_j(t, \mathbf{x}, \mathbf{z})|}{a^*} \right\} \tag{28}$$

where $\delta u_j(t, \mathbf{x}, \mathbf{z}), j = 1, 2$, are the interstory drifts, $a_j(t, \mathbf{x}, \mathbf{z}), j = 1, 2$, are the total accelerations at the first and second floor, respectively, and $\delta^* = 0.42$ and $a^* = 0.84$ are the acceptable response levels. The failure probability function $P_F(\mathbf{x})$ can be written in terms of the demand function as the multidimensional probability integral

$$P_F(\mathbf{x}) = \int_{d(\mathbf{x}, \mathbf{z}) > 1} p(\mathbf{z}) d\mathbf{z} \tag{29}$$

where $p(\mathbf{z})$ is the joint probability density function of the uncertain parameters involved in the characterization of the excitation. This function indicates the relative plausibility of the possible values of the uncertain parameters $\mathbf{z} \in \mathbf{Z}$. It is noted that the above multidimensional probability integral involves more than 1000 random variables in this case (see Section 5.3.1). Therefore, the reliability estimation for a given design constitutes a high-dimensional problem as previously pointed out [32, 40, 41].

8. Appendix B

The failure event associated with the interstory displacement of the first floor is given by

$$F_1(\mathbf{x}, \mathbf{z}) = \max_{t \in [0, t_T]} \left\{ \frac{|u_x^1(t, \mathbf{x}, \mathbf{z})|}{u^{1^*}}, \frac{|u_y^1(t, \mathbf{x}, \mathbf{z})|}{u^{1^*}} \right\} > 1 \tag{30}$$

where $u_x^1(t,\mathbf{x},\mathbf{z})$ and $u_y^1(t,\mathbf{x},\mathbf{z})$ are the centroid relative displacements of the first floor along the x and y direction, respectively, and u^{1^*} is the maximum allowable drift equal to 0.08% of the first story height.

The failure event related to the roof displacement is given by

$$F_2(\mathbf{x},\mathbf{z}) = \max_{t\in[0,t_T]}\left\{\frac{|u_x^2(t,\mathbf{x},\mathbf{z})|}{u^{2^*}},\frac{|u_y^2(t,\mathbf{x},\mathbf{z})|}{u^{2^*}}\right\} > 1 \tag{31}$$

where $u_x^2(t,\mathbf{x},\mathbf{z})$ and $u_y^2(t,\mathbf{x},\mathbf{z})$ are the centroid displacements at the top of the building along the x and y direction, respectively, and u^{2^*} is the maximum allowable roof displacement equal to 0.075% of the building height. As in the Application 1, the reliability estimation for a given design constitutes a high-dimensional problem. In fact, more than 1500 random variables are involved in the corresponding multidimensional probability integral in this case.

9. Appendix C

A kriging-based model is selected for approximating the failure probability functions [42, 43]. Validation calculations have shown that it is computationally more stable and efficient to perform the kriging interpolation in the physical design space $\mathbf{X}$ rather than in the underlying normal space $\mathbf{Y}$ [17]. Furthermore, it is more convenient, from the numerical point of view, to approximate the logarithm of the failure probability function than the failure probability function itself [44]. In this framework, the idea is to construct an initial data-base of support points during the first stage of Phase I which is updated during the different stages of the proposed approach. The support points are then used to construct the kriging estimates of the logarithm of the failure probability functions, i.e., $P_{F_i}^{Ln}(\mathbf{x}) = \ln(P_{F_i}(\mathbf{x}))$. The numerical implementation is as follows.

1) The initial set of support points and the corresponding values of $P_{F_i}^{Ln}(\mathbf{x})$ are generated during the first stage of Phase I. This implies a direct evaluation of $P_{F_i}^{Ln}(\mathbf{x})$ at the support points. Define the number of support points n_{su}, and error tolerance level ϵ.

2) For a given candidate sample $\mathbf{x}^{\text{new}}$, find its closest n_{su} support points according to, e.g., the Euclidean distance.

3) Check if $\mathbf{x}^{\text{new}}$ belongs to the n_d-dimensional convex hull of the support points. If not, go to step 6.

4) Estimate the coefficient of variation of the kriging estimate. Check the variability of the estimate. If its coefficient of variation is greater than the error tolerance level ϵ, go to 6.

5) Kriging estimate of $P_{F_i}^{Ln}(\mathbf{x})$ is accepted for the candidate sample $\mathbf{x}^{\text{new}}$. Go to step 7.

6) Evaluate $P_{F_i}^{Ln}(\mathbf{x}^{\text{new}})$ directly from the physical model. Store the values of $\mathbf{x}^{\text{new}}$ and $P_{F_i}^{Ln}(\mathbf{x}^{\text{new}})$ in the database of support points.

7) Continue with the updating process.

This procedure is repeated during the different stages of the proposed Two-Phase method. For more details about the implementation of the meta-model, the reader is referred to [17, 29, 45].

References

[1] R.T. Haftka and Z. Gurdal. Elements of structural optimization. 3rd ed. *Dordrecht: Kluwer Academic Publishers*, 1992.

[2] J.S. Arora. Introduction to optimum design. 4th ed. Elsevier, 2017.

[3] T.H. Holland. Adaptation in natural and artifficial systems. *University of Michigan Press*, Ann Arbor, Michigan, 2003.

[4] S. Kirkpatrick, C. D. Gelatt and M. P. Vecchi. Optimization by simulated annealing. *Science*, 220(4598):165–172, 1983.

[5] J. Kennedy and R. C. Eberhart. Characteristic mode based component mode synthesis for power flow analysis in complex structures. *Proceedings of IEEE International Conference on Neural Networks*, Vol. 4, 165–172, 1995.

[6] V. Maniezzo, M. Dorigo and N. Colorni. The ant system: Optimization by a colony of cooperating agents. *IEEE Transactions on Systems, Man and Cybernetics - Part B*, 26(1):29–41, 1996.

[7] F. Liang. Annealing evolutionary stochastic approximation Monte Carlo for global optimization. *Statistics and Computing*, 21:113-119, 2011.

[8] C.A. Coello Coello and E.M. Montes. Constraint-handling in genetic algorithms through the use of dominance-based tournament selection. *Ad. Eng. Inform.*, 16(3):193-203, 2002.

[9] Y. Dong, J. Tang, B. Xu and D. Wang. An application of swarm optimization to nonlinear programming. *Computers & Mathematics with Applications*, 49(11-12):1655-1668, 2005.

[10] E. Mezura-Montes and C.A. Coello Coello. Use of multi-objective optimization concepts to handle constraints in genetic algorithms. *In: Abraham A, Jain L, Goldberg R, editors. Evolutionary multi-objective optimization.* Berlin, Springer, 2005.

[11] Z. Michalewicz. Evolutionary algorithms for constrained parameter optimization problems. *Evolutionary Computation*, 4(1):132, 1996.

[12] A. Hedar and M. Fukushima. Derivative-free filter simulated annealing method for constrained continuous global optimization. *Journal of Global Optimization*, 35(4):521549, 2006.

[13] L.J. Li, Z. Huang, F. Liu and Q.H. Wu. A heuristic particle swarm optimizer for optimization of pin connected structures. *Computers and Structures*, 85(78):340349, 2007.

[14] H.-S. Li and S.-K. Au. Design optimization using subset simulation algorithm. *Structural Safety*, 32:384-392, 2010.

[15] J. Ching and Y.C. Chen. Transitional Markov chain Monte Carlo method for Bayesian updating, model class selection, and model averaging. *Journal of Engineering Mechanics*, 133:816–832, 2007.

[16] W. Betz, I. Papaioannou and D. Straub. Transitional Markov chain Monte Carlo: Observations and improvements. *Journal of Engineering Mechanics*, 142(5):04016016, 2016.

[17] H. A. Jensen, D. J. Jerez and M. Valdebenito. An adaptive scheme for reliability-based global design optimization: A Markov chain Monte Carlo approach. *Mechanical Systems and Signal Processing*, 143:106836, 2020.

[18] P. Angelikopoulos, C. Papadimitriou, and P. Koumoutsakos. Bayesian uncertainty quantification and propagation in molecular dynamics simulations: a high performance computing framework. *The Journal of Chemical Physics*, 137:1441103-1–144103-19, 2012.

[19] H.A. Jensen, E. Millas, D.Kusanovic, C. Papadimitriou. Model reduction techniques for Bayesian finite element model updating using dynamic response data. *Computer Methods in Applied Mechanics and Engineering*, 279:301-324, 2014.

[20] J.L. Beck. Bayesian system identification based on probability logic. *Structural Control and Health Monitoring*, 17(7):825–847, 2010.

[21] E.N. Chatzi and C. Papadimitriou (eds.). Identification Methods for Structural Health Monitoring. Series: CISM-International Centre for Mechanical Sciences. *Springer*, Berlin, Germany, 2016.

[22] K. V. Yuen. Bayesian methods for structural dynamics and civil engineering. *John Wiley & Sons*, 2010.

[23] K. M. Zuev and J.L. Beck. Global optimization using the asymptotically independent Markov sampling method. *Computers and Structures*, 126:107–119, 2013.

[24] J. Wang and L.S. Katafygiotis. Reliability-based optimal design of linear structures subjected to stochastic excitations. *Structural Safety*, 47:29–38, 2014.

[25] A. Kong, J. S. Liu and W. H. Wong. Sequential imputations and Bayesian missing data problems. Journal of the American Statistical Association, 89(425):278–288, 1994.

[26] J. S. Liu. Metropolized independent sampling with comparison to rejection sampling and importance sampling. Statistics and Computing, 6(2):113–119, 1996.

[27] N. Metropolis, A. Resenbluth, M. Resenbluth, A. Teller and E. Teller. Equations of state calculations by fast computing machines. *Journal of Chemical Physics*, 21(6):1087–1092, 1953.

[28] W. Hastings. Monte Carlo sampling methods using Markov chains and their applications. *Biometrika*, 57(1):97–109, 1970.

[29] H.A. Jensen, C. Esse, V. Araya and C. Papadimitriou. Implementation of an adaptive meta-model for Bayesian finite element model updating in time domain. *Reliability Engineering & System Safety*, 160:174–190, 2017.

[30] M.F. Pellissetti. Parallel processing in structural reliability. Journal of Structural Engineering and Mechanics, 32(1):95–126, 2009.

[31] D.M. Moore. Simulation of ground motion using the stochastic method. *Pure and Applied Geophysics*, 160:635–676, 2003.

[32] S.-K. Au and J.L. Beck. Estimation of small failure probabilities in high dimensions by subset simulation. *Probabilistic Engineering Mechanics*, 16(4):263–277, 2001.

[33] G.M. Atkinson and W. Silva. Stochastic modeling of California ground motions. *Bulletin of the Seismological Society of America*, 90(2):255–274, 2000.

[34] G.P. Mavroeidis. A Mathematical Representation of Near-Fault Ground Motions *Bulletin of the Seismological Society of America*, 93(3):1099–1131, 2003.

[35] Q. He and L. Wang. An effective co-evolutionary particle swarm optimization for constrained engineering design problems. *Eng. Appl. Artif. Intel.*, 20(1):89-99, 2007.

[36] Q. He and L. Wang. A hybrid particle swarm optimization with a feasibility-based rule for constrained optimization. *Appl. Math. Compt.*, 186(2):1407-1422, 2007.

[37] C.A. Coello Coello. Use of a self-adaptive penalty approach for engineering optimization problems. *Comput Ind.*, 41(2):13-27, 2000.

[38] K.S. Lee, Z.W. Geem. A new structural optimization method based on the harmony search

algorithm. *Computers and Structures*, 82(9-10):781-798. 2004.

[39] H. J. Pradlwarter and G. I. Schuëller. Equivalent linearization – A suitable tool for analyzing MDOF-systems. Probabilistic Engineering Mechanics, 8(2):115–126, 1993.

[40] P.S. Koutsourelakis, H.J. Pradlwarter and G.I. Schuëller. Reliability of structures in high dimensions, part I: Algorithms and applications. *Probabilistic Engineering Mechanics*, 19(4):409–417, 2004.

[41] J. Li and J.B. Chen. Stochastic dynamics of structures. *John Wiley and Sons.*, Singapore, 2009.

[42] T. Santner, B. Williams, W. Notz. The design and analysis of computer experiments. *Springer*, 2003.

[43] S.N. Lophaven, H.B. Nielsen and J. Søndergaard. DACE: A MATLAB Kriging Toolbox,. DTU. Lyngby, Denmark, 2002.

[44] M. Gasser and G.I. Schuëller. Reliability-based optimization of structural systems. *Mathematical Methods of Operational Research*, 46(3):287–307, 1997.

[45] P. Angelikopoulus, C. Papadimitriou, P. Koumoutsakos. X-TMCMC:Adaptive kriging for Bayesian inverse modeling. *Computer Methods in Applied Mechanics and Engineering*, 289:409–428, 2015.